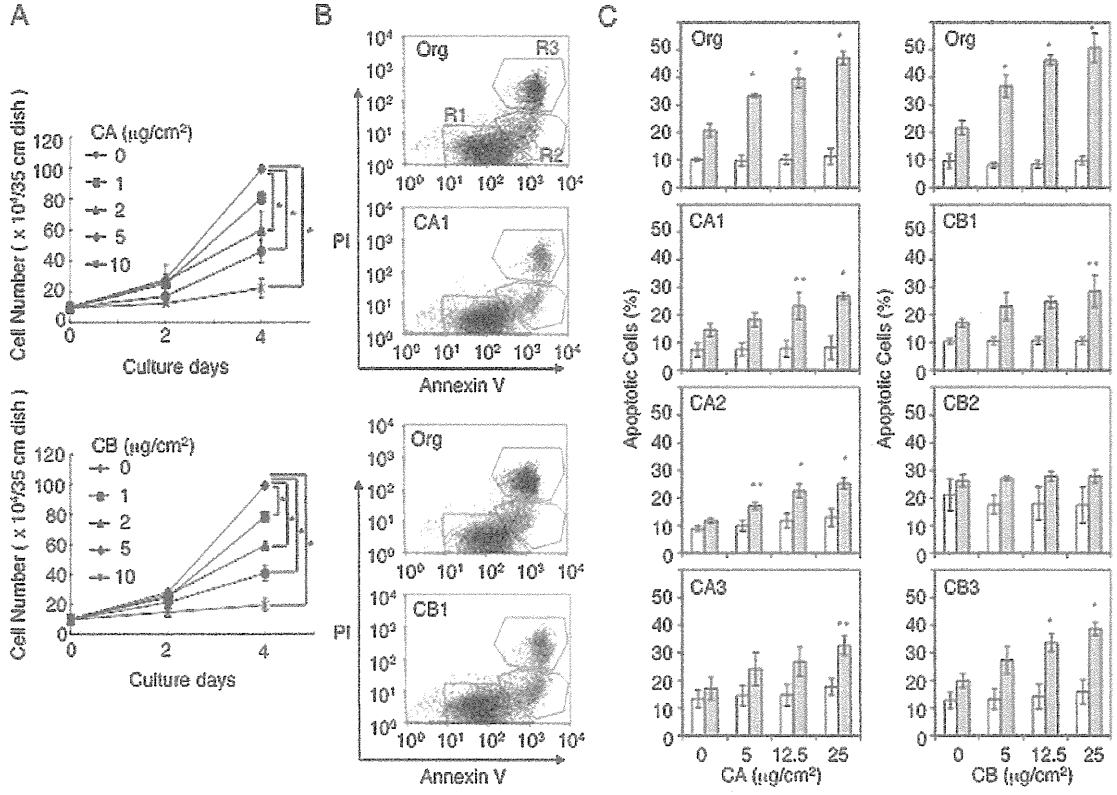

Figure 2. Original MT-2 (MT-2Org) cells acquire resistance to chrysotile-induced apoptosis by long-term and low-level exposures to chrysotile. (*A*) MT-2Org (Org) cells (1×10^5/2 ml) were cultured in the absence or presence of 1, 2, 5, or 10 μg/cm² chrysotile-A (CA) (*top*) or CB (*bottom*) in a 35-mm dish for 2 or 4 days. The number of viable cells was determined using the trypan blue dye exclusion test. (*B, C*) MT-2Org and MT-2Rsts (CA1, CA2, CA3, CB1, CB2, and CB3) cells (1×10^5/ml) were cultured in the absence or presence of 5, 12.5, or 25 μg/cm² CA or CB in 24-well plates. After 24 hours, apoptotic cells were detected by staining with Annexin V–FITC and propidium iodide, and stained cells were analyzed using FACS (FACS profiles shown in *B*). Region 1 (R1) represents viable cells (Annexin V-/PI-). Region 2 (R2) contains early apoptotic cells (Annexin V+/PI-). Region 3 (R3) includes late apoptotic cells (Annexin V+/PI+). (*C*) Percentages of apoptotic cells. *Open bars* and *gray bars* show (R2/(R1 + R2 + R3)) and ((R2 + R3)/(R1 + R2 + R3)), respectively. Data shown are the mean ± SD of three independent experiments. *P* values were obtained using Dunnett's test. $^*P < 0.01$. $^{**}P < 0.05$.

Statistical Analysis

Dunnett's test was performed to determine statistical differences between each experimental group and the control group.

RESULTS

Establishment of Six MT-2Rsts Cells (CA1–3 and CB1–3)

As we reported previously (17, 18), we initially established CB1 cells. Therefore, the other five independent MT-2Rsts cells continuously exposed to CA or CB were established according to a similar method. As shown in Figure 2A, the growth of MT-2Org cells was inhibited in a dose-dependent manner by culturing with CA or CB. This growth inhibition was confirmed by the appearance of apoptosis, as reported previously (17, 18), and as demonstrated in Figures 2B and 2C. All cultures for the establishment of MT-2Rsts cells were initiated in the presence of 2 μg/cm² CA or CB, at which stage the proliferation of MT-2Org cells was inhibited by half (Figure 2A). After 8–12 months of culture with CA or CB, MT-2Rsts cells began to exhibit a reduced apoptotic fraction when these cells were cultured with various concentrations of CA or CB (Figure 2C). Thus, we determined that six MT-2Rsts cells representing the acquisition of resistance to asbestos-induced apoptosis had been established, and these cells were designated CA1–3 and CB1–3. In this study, to identify those genes involved in the reduction of antitumor immune functions induced by exposure to asbestos, we used these six MT-2Rsts cells for DNA microarray analysis.

Gene Expression in MT-2Rsts Cells Altered by Chronic Exposure to Chrysotile

To examine alterations in gene expression by chronic exposure to chrysotile, DNA microarray analysis was performed with MT-2Org and MT-2Rsts cells. As listed in Table 1, the expression of 139 genes was altered (84 were up-regulated, and 55 were down-regulated) significantly (greater than twofold changes), and most were categorized in cellular components, biological processes, and molecular function groups by gene ontology analysis (data not shown). As shown in Figure 3, clustering analysis using these 139 genes revealed that the gene expression pattern was obviously different between MT-2Org and MT-2Rsts cells, and gene expression patterns were similar among all six MT-2Rsts cells, although small differences were evident. These results indicated that the changes in gene expression of MT-2Org cells are similarly induced by chronic exposure to CA and CB, suggesting that MT-2Rsts cells would be useful in further analyzing the immunologic effects of chrysotile asbestos.

Pathway and Network Analysis Using the MetaCore System

In an effort to identify genes related to the suppression of antitumor immunity among the 139 genes identified, expression

TABLE 1. GENES WITH AT LEAST A TWOFOLD DIFFERENCE BETWEEN MT-2ORG AND MT-2RSTS AT $P < 0.05$

Description	Genes	Accession Numbers
Down-regulated in MT-2Rsts compared with MT-2Org		
Solute carrier family 15, member 3	*SLC15A3*	NM_016582
Stomatin	*STOM*	NM_198194
Nedd4 family interacting protein 1	*NDFIP1*	NM_030571
Creatine kinase, brain	*CKB*	NM_001823
Tripartite motif–containing 22	*TRIM22*	NM_006074
Apolipoprotein C–I	*APOC1*	NM_001645
Forkhead box O1	*FOXO1*	NM_002015
Chromosome 1 open reading frame 218	*C1orf218*	NM_019049
Solute carrier family 6 (neurotransmitter transporter, taurine), member 6	*SLC6A6*	AB209172
c-mer proto-oncogene tyrosine kinase	*MERTK*	NM_006343
Interferon regulatory factor 9	*IRF9*	NM_006084
Asparaginase-like–1	*ASRGL1*	BC021295
Ankyrin repeat and death domain–containing 1A	*ANKDD1A*	AK075298
Protein phosphatase 1, regulatory (inhibitor) subunit 16B	*PPP1R16B*	NM_015568
Secreted protein, acidic, cysteine-rich (osteonectin)	*SPARC*	NM_003118
Chromosome 5 open reading frame 30	*C5orf30*	NM_033211
Stromal antigen 3	*STAG3*	NM_012447
Apolipoprotein L, 6	*APOL6*	AK074645
Chromosome 5 open reading frame 40	*C5orf40*	NM_001001343
CXXC finger 5	*CXXC5*	NM_016463
RNase, RNase A family, 1 (pancreatic)	*RNASE1*	NM_198232
Eukaryotic translation initiation factor 4 γ, 3	*EIF4G3*	NM_003760
Leukemia inhibitory factor (cholinergic differentiation factor)	*LIF*	NM_002309
Radial spoke head 1 homologue (*Chlamydomonas*)	*RSPH1*	NM_080860
cDNA DKFZp564D0472	*TOMM22*	AL110179
X-linked Kx blood group (McLeod syndrome)	*XK*	NM_021083
Caspase 2 and receptor-interacting serine-threonine kinase 1 domain containing adaptor with death domain	*CRADD*	NM_003805
Chromosome 13 open reading frame 15	*C13orf15*	NM_014059
An acute myeloid leukemia protein (486 bp)	*aml1*	X90980
Serine propidium iodide Kazal type 5–like 3	*SPINK5L3*	AK001520
Transmembrane and coiled-coil domain family 2	*TMCC2*	NM_014858
Von Willebrand factor	*VWF*	NM_000552
Acid phosphatase–like 2	*ACPL2*	NM_152282
Interferon-induced protein with tetratricopeptide repeats 2	*IFIT2*	NM_001547
Chemokine (C-C motif) ligand 4	*CCL4*	NM_002984
Napsin A aspartic peptidase	*NAPSA*	NM_004851
Hypothetical gene supported by AK125122	*FLJ13137*	AK125122
G-protein–coupled receptor 56	*GPR56*	NM_201525
Zinc finger CCCH-type containing 12D	*ZC3H12D*	AK127932
Similar to ciliary rootlet coiled-coil, rootletin	*LOC285188*	XM_209505
Membrane-associated ring finger (C3HC4) 3	*MARCH3*	NM_178450
Sequence 155 from Patent WO0220754	*AX721195*	AX721195
Protein kinase C, β1	*PRKCB1*	NM_002738
Interleukin 28A (interferon, λ2)	*IL28A*	NM_172138
DKFZP564O0823 protein	*DKFZP564O0823*	NM_015393
AF032119 hCASK {*Homo sapiens*;}, partial (13%)	*THC2443571*	THC2443571
Chromosome 19 open reading frame 38	*C19orf38*	XM_172995
Chemokine (C-X-C motif) receptor 3	*CXCR3*	NM_001504
Sema domain, transmembrane domain (TM), and cytoplasmic domain, (semaphorin) 6A	*SEMA6A*	NM_020796
Deleted in esophageal cancer 1	*DEC1*	BC030567
Phosphatidylinositol 3,4,5-trisphosphate–dependent Ras-related C3 botulinum toxin substrate 1 exchanger 1	*PREX1*	NM_020820
Breast cancer antiestrogen resistance 3	*BCAR3*	NM_003567
Myeloid cell nuclear differentiation antigen	*MNDA*	NM_002432
Integrin, β7	*ITGB7*	NM_000889
Hypothetical protein LOC199725	*LOC199725*	AK023628
Up-regulated in MT-2Rsts compared with MT-2Org		
Hypothetical LOC728701	*LOC728701*	BC011779
Mediator complex subunit 19	*MED19*	NM_153450
Norrie disease (pseudoglioma)	*NDP*	NM_000266
Protein phosphatase 6, regulatory subunit 1	*SAPS1*	NM_014931
Phosphoprotein enriched in astrocytes 15	*PEA15*	NM_003768
cDNA clone: 6386006	*BU587941*	BU587941
Hypothetical protein FLJ11348	*AK002210*	AK002210
FLJ00217 protein	*AK074144*	AK074144
cDNA clone: 5451514	*BM045853*	BM045853
F-box protein 2	*FBXO2*	NM_012168
cDNA clone: 1917130	*SSR2*	AI344752
AF4/FMR2 family, member 3	*AFF3*	NM_002285
Breakpoint cluster region	*BCR*	NM_021574
cDNA clone CS0DM002YA18	*CR608907*	CR608907

(*Continued*)

TABLE 1. (CONTINUED)

Description	Genes	Accession Numbers
Myc associated factor X dimerization protein 1	*MXD1*	NM_002357
cDNA MR0-RT0026-160401-104-h09 RT0026	*BI009763*	BI009763
Glutamate receptor interacting protein and coiled-coil domain containing 2	*GCC2*	NM_181453
Transmembrane emp24-like trafficking protein 10 (yeast) pseudogene	*TMED10P*	AJ004914
Special AT-rich sequence-binding protein homeobox 1	*SATB1*	NM_002971
Zinc finger CCCH-type containing 7A	*ZC3H7A*	NM_014153
Toll interacting protein	*TOLLIP*	NM_019009
cDNA FLJ13707 fis, clone PLACE2000347	*STAMBP*	AK023769
Ninein (GSK3B interacting protein)	*NIN*	NM_016350
Melanoma inhibitory activity family, member 3	*MIA3*	AK096526
Ras-related protein 1 GTPase-activating protein	*RAP1GAP*	NM_002885
Elongation factor Tu GTP binding domain containing 1	*EFTUD1*	NM_024580
Suppressor of Ty, domain containing 1 (*Saccharomyces cerevisiae*)	*SPTY2D1*	NM_194285
Hepatoma-derived growth factor, related protein 3	*HDGFRP3*	NM_016073
RNA binding motif protein 22	*RBM22*	NM_018047
Calcium/calmodulin-dependent serine protein kinase interacting protein 2	*CASKIN2*	NM_020753
Ras association (RalGDS/AF-6) and pleckstrin homology domains 1	*RAPH1*	NM_213589
Hypothetical protein LOC286272	*LOC286272*	AK000939
Transmembrane protease, serine 3	*TMPRSS3*	NM_032401
Coiled-coil domain containing 66	*CCDC66*	NM_001012506
Solute carrier family 45, member 4	*SLC45A4*	AB032952
cDNA clone: 3948082	*NOS1*	BC010126
Iroquois homeobox 5	*IRX5*	NM_005853
Organic solute transporter–β	*OSTbeta*	NM_178859
Hypothetical protein FLJ10404	*FLJ10404*	NM_019057
Regulating synaptic membrane exocytosis 3	*RIMS3*	NM_014747
Chorionic gonadotropin, β-polypeptide 1	*CGB1*	NM_033377
Secreted frizzled-related protein 1	*SFRP1*	NM_003012
Cysteine-rich secretory protein Limulus factor C, Coch-5b2 and Lgl1 domain–containing 2	*CRISPLD2*	BC007689
Protein phosphatase 1F (PP2C domain containing)	*PPM1F*	NM_014634
Steroidogenic acute regulatory protein-related lipid transfer (START) domain–containing 13	*STARD13*	NM_178006
Phospholipase C, β2	*PLCB2*	NM_004573
Glucosyltransferases, Rab-like GTPase activators and Myotubularins domain–containing 1C	*GRAMD1C*	NM_017577
cDNA clone: 998I221826	*BX119852*	BX119852
Replication protein A4, 34 kD	*RPA4*	NM_013347
Calcium-binding protein 7	*CABP7*	NM_182527
Golgin-like hypothetical protein LOC440321	*FLJ32679*	NM_001012452
Leucine-rich repeat–containing 2	*LRRC2*	NM_024512
Solute carrier family 10 (sodium/bile acid cotransporter family), member 1	*SLC10A1*	NM_003049
Tryptophan-aspartic acid repeat domain 33	*WDR33*	NM_018383
cDNA clone: 277235	*N47124*	N47124
Phosphoinositide-3–kinase, regulatory subunit 5	*PIK3R5*	NM_014308
Insulin-like growth factor binding protein 3	*IGFBP3*	NM_001013398
Dystrophin	*dystrophin*	S71486
Growth factor receptor bound protein 2-associated binding protein 2	*GAB2*	NM_012296
Carbonic anhydrase II	*CA2*	NM_000067
A kinase anchor protein 12	*AKAP12*	NM_144497
cDNA clone: 450936	*AA704712*	AA704712
Insulin-like growth factor 2 mRNA binding protein 2	*IGF2BP2*	NM_006548
Cystatin A (stefin A)	*CSTA*	NM_005213
Septin 1	*SEPT1*	NM_052838
Tight junction protein 1 (zona occludens 1)	*TJP1*	NM_003257
Coiled-coil domain containing 88A	*CCDC88A*	NM_018084
cDNA DKFZp686J1595	*BX538057*	BX538057
Chromosome 5 open reading frame 39	*C5orf39*	NM_001014279
Calcium-binding protein 39-like	*CAB39L*	NM_030925
Transmembrane protein 56	*TMEM56*	NM_152487
Tryptophan-tryptophan domain containing oxidoreductase	*WWOX*	NM_130844
FLJ35767 protein	*FLJ35767*	NM_207459
Riboflavin kinase	*RFK*	NM_018339
Stress-associated endoplasmic reticulum protein family member 2	*SERP2*	NM_001010897
Dehydrogenase/reductase member 9	*DHRS9*	NM_005771
Teashirt zinc finger homeobox 1	*TSHZ1*	NM_005786
Nance-Horan syndrome-like 1	*NHSL1*	AB037778
Solute carrier family 39 (zinc transporter), member 6	*SLC39A6*	NM_012319
Zinc finger, Cysteine-cysteine-histidine-cysteine domain–containing 2	*ZCCHC2*	BC006340
Zinc-binding alcohol dehydrogenase domain–containing 2	*ZADH2*	NM_175907
Pentraxin-related gene, rapidly induced by IL-1β	*PTX3*	NM_002852
Family with sequence similarity 124B	*FAM124B*	NM_024785
Forkhead box F2	*FOXF2*	NM_001452

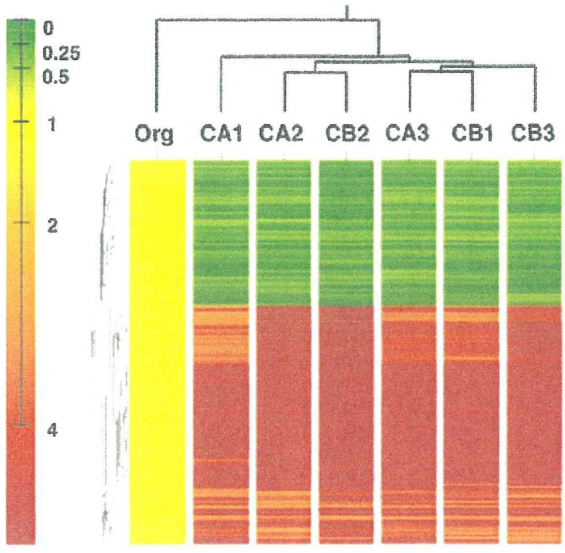

Figure 3. Clustering analysis of 139 genes reveals differences between MT-2Org and MT-2Rsts cells. Expression is scaled so that *green* represents low expression, and *red* represents high expression.

data were processed by the MetaCore system, which allows the visualization of microarray data on canonical pathways and the construction of gene networks using pathway and network analysis. The top 30 results of the pathway analysis are listed in Table 2. We focused on the suppression of the IFN-γ signaling pathway, because the production of IFN-γ was shown to decrease in CB1 cells compared with MT-2Org cells (17), and IFN-γ is considered one of the most important cytokines for organizing tumor rejection by immunocompetent cells. The expression of two genes, IFN regulatory factor 9 (*IRF9*) and IFN-stimulated gene factor–3 (*ISGF3*), was significantly reduced in all MT-2Rsts cells exposed continuously to CA or CB (Figure 4). In addition, the build networks from the 139 genes indicated that the decreased expression of CXCR3 in all MT-2Rsts cells was regulated by *IRF9* through CXCL10/IP-10 (Figure 5). Therefore, the cell-surface expression of CXCR3 was thought to be important among the cellular and molecular alterations in MT-2Rsts cells continuously exposed to asbestos.

Decline of Th1-Type CXCR3 Expression, IFN-γ Production, and CXCL10/IP10 Production in MT-2Rsts Cells Chronically Exposed to Chrysotile Asbestos

Because the expression of CXCR3 and production of IFN-γ are known to be induced by T-cell activation and lead to the enhancement of antitumor immune function (22), we investigated the expression of the Th1-type chemokine receptor CXCR3 and cytokine IFN-γ. As shown in Figure 6A, the cell-surface expression of CXCR3 was examined in gated live cells on MT-2Org and MT-2Rsts cells. All MT-2Rsts cells showed a reduction of cell-surface CXCR3-positive cells, although no significant difference was evident between MT-2Org and CB2 cells, as indicated by real-time RT-PCR (Figure 6B). Furthermore, all MT-2Rsts cells showed less production of IFN-γ compared with MT-2Org cells (Figure 7A). These findings support the notion that the down-regulation of Th1-type molecules CXCR3 and IFN-γ is important in recognizing the immunologic effect of asbestos.

As shown in Figure 7B, the production of the Th1-type CXCR3 ligand CXCL10/IP10 was also significantly reduced in all MT-2Rsts cells compared with MT-2Org cells. In addition, another Th1-type chemokine, *CCL4/ MIP-1β* mRNA, was also expressed at low concentrations in all MT-2Rsts cells compared

TABLE 2. PATHWAY RESULTS

Map	*P* values[a]
1. Phosphatidylinositol-3,4,5-trisphosphate signaling in B lymphocytes	5.22E-03
2. IFN-α/β signaling pathway	9.05E-03
3. Regulation of lipid metabolism G–α(q) regulation of lipid metabolism	1.55E-02
4. Inhibitory action of lipoxins on superoxide production in neutrophils	1.95E-02
5. Angiotensin signaling via signal transducers and activators of transcription	1.95E-02
6. Transcription factor Tubby signaling pathways	2.62E-02
7. Transcription regulation of granulocyte development	3.46E-02
8. Apoptosis and survival–β-2 adrenergic receptor antiapoptotic action	4.71E-02
9. Membrane trafficking and signal transduction of G-α (i) heterotrimeric G-protein	5.30E-02
10. Gap junctions	9.35E-02
11. G-protein–β/γ signaling cascades	1.01E-01
12. Macrophage migration inhibitory factor, the neuroendocrine-macrophage connector	1.32E-01
13. α-2 adrenergic receptor regulation of ion channels	1.40E-01
14. Antiviral actions of interferons	1.65E-01
15. Calcium signaling	1.74E-01
16. Extracellular signal–regulated kinase interactions: inhibition of extracellular signal–regulated kinases	1.82E-01
17. G-protein–mediated regulation mitogen-activated protein kinase-extracellular signal–regulated kinase signaling	1.91E-01
18. Endothelin receptor type B signaling	1.91E-01
19. A1 receptor signaling	2.00E-01
20. A3 receptor signaling	2.00E-01
21. G-protein–mediated regulation p38 and c-Jun N-terminal kinase signaling	2.00E-01
22. Inducible costimulator-Inducible costimulator ligand pathway in T-helper cells	2.09E-01
23. Histamine H1 receptor signaling in the interruption of cell-barrier integrity	2.17E-01
24. Inhibitory action of lipoxins on neutrophil migration	2.17E-01
25. Histamine signaling in dendritic cells	2.35E-01
26. Activation of protein kinase C via G-protein–coupled receptor	2.35E-01
27. Inositol 1,4,5-triphosphate signaling	2.44E-01
28. Role of vitamin D receptor in regulation of genes involved in osteoporosis	2.80E-01
29. IFN-γ signaling pathway	2.89E-01
30. G protein-coupled receptors in platelet aggregation	3.42E-01

[a]*P* values is calculated by comparing the number of interest genes that participate in a given pathway, relative to the total number of occurrences of these genes in all pathway annotations stored in the Metacore database.

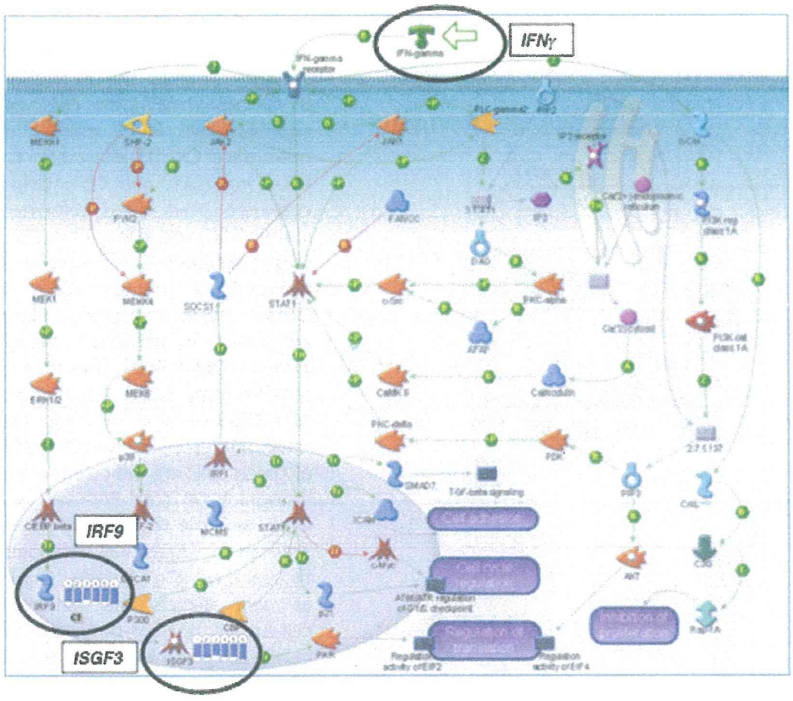

Figure 4. IFN-γ signaling canonical pathway analysis shows that the expression of *IRF9* and *ISGF3* is down-regulated in MT-2Rsts cells. *Blue thermometers* indicate down-regulation. Numbers indicate cell line names (2, CA1; 3, CA2; 4, CA3; 5, CB1; 6, CB2; 7, CB3).

with MT-2Org cells (Table 1 and Figure 7C). However, CCR5, the Th1-type receptor for CCL4/MIP-1β, was not reduced significantly through the expression of mRNA in MT-2Rsts cells (Figure 7C). These results indicate that a continuous exposure of MT-2Org cells to asbestos altered the expression of Th1-related chemokines (CXCL10/IP10 and CCL4/MIP-1β) and chemokine receptors (CXCR3).

DISCUSSION

Pneumoconiosis is an occupational and restrictive set of lung diseases caused by the inhalation of dust, often in mines (23–26), and typically including silicosis and asbestosis. Silicosis is caused by the inhalation of crystalline silica dust, and is marked by inflammation and scarring in the form of nodular lesions in the upper lobes of lungs. On the other hand, asbestosis is a chronic inflammatory and fibrotic medical condition affecting the parenchymal tissue of the lungs, and is caused by the inhalation and retention of asbestos fibers. It usually occurs after high-intensity or long-term exposure to asbestos, particularly in individuals working on the production or end-use of products containing asbestos (23–26). Patients with silicosis suffer not only from respiratory dysfunction, but sometimes from complications involving autoimmune diseases such as rheumatoid arthritis

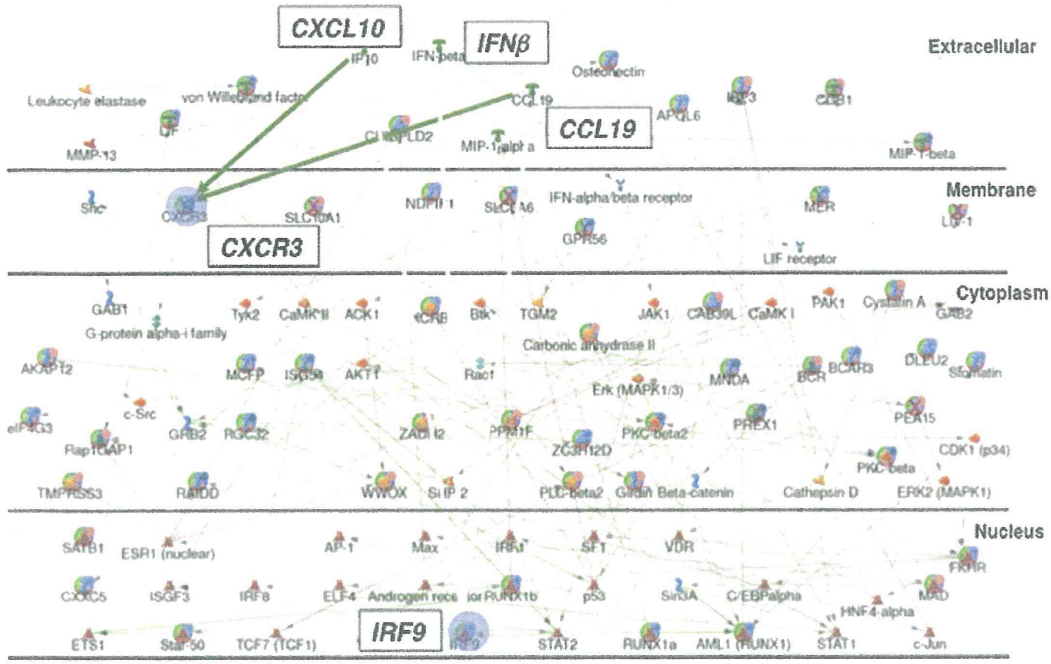

Figure 5. Network analysis indicates that down-regulation of *CXCR3* is regulated by *IRF9*. *Blue circles* indicate reduced genes. *Green arrows* and *gray arrows* indicate positive and unspecified effects, respectively.

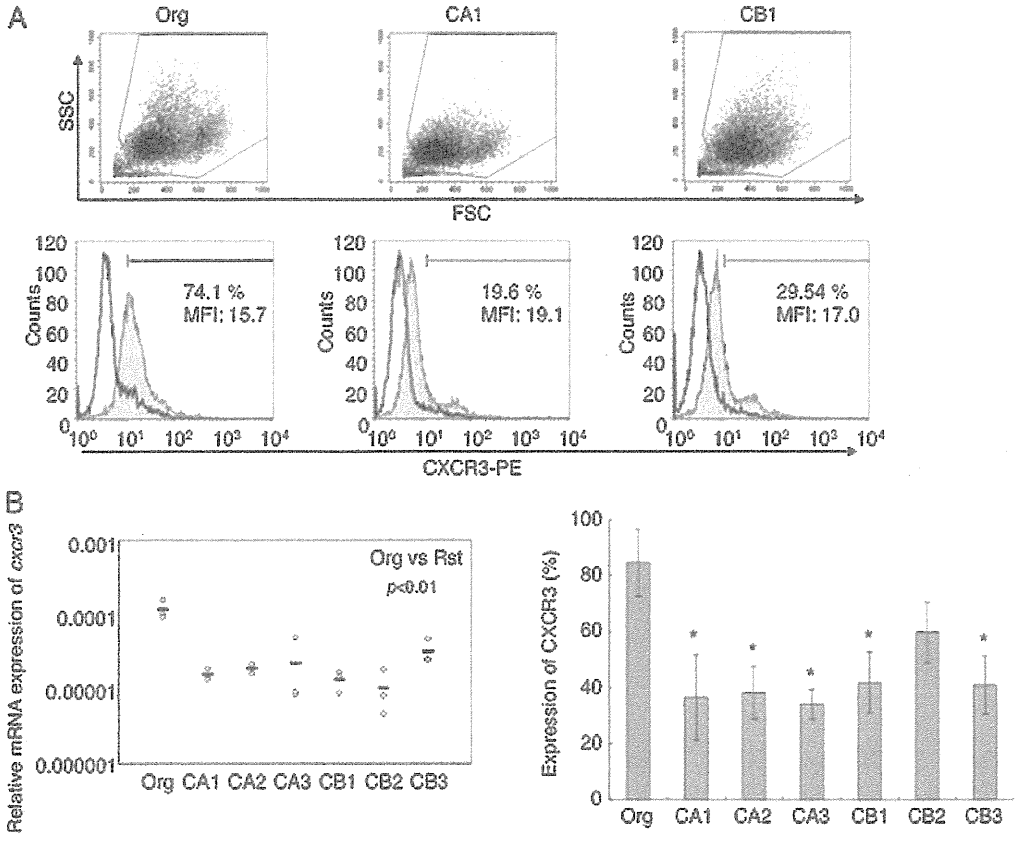

Figure 6. Chronic exposure to chrysotile inhibits the expression of CXCR3 in MT-2Rsts cells. (*A*) Representative FACS profiles of cell-surface CXCR3 expression on MT-2Org, CA1, and CB1. Living cells were gated, based on forward scatter (FSC) and side scatter (SSC) (*upper dot plot*). Gated cells were analyzed for the expression of CXCR3 (*lower histogram*). Peaks are shown in unstained control samples (*solid lines*) and stained samples (*gray peaks*). Percentages of CXCR3-positive cells and the mean fluorescence intensity (MFI) of gated cells are indicated in the histogram. (*B*) Total RNA was isolated, and the relative mRNA expression of *CXCR3* was estimated by real-time RT-PCR (*left*). Graph at *right* depicts the ratios of cell-surface CXCR3-positive cells in MT-2Org and MT-2Rsts. Results represent the mean ± SD of three independent experiments. *P* values were obtained using Dunnett's test. $*P < 0.01$. $**P < 0.05$.

(known as Caplan's syndrome), systemic sclerosis, and antineutrophil cytoplasmic autoantibody–related vasculitis/nephritis (26–28). However, the most important complication in patients exposed to asbestos involves the occurrence of cancers, such as lung cancer and MM. In particular, MM is known to be caused by low-level and long-term exposures to asbestos (29–31).

We have been studying the mechanisms of dysregulation of autoimmunity caused by exposure to silica, and reported on alterations in Fas/CD95 and related molecules (32, 33), the activation of T cells by silica via the activation of antigen-presenting cells such as dendritic cells and monocyte/macrophage-lineage cells (34), and a reduction of regulatory T-cell function in the peripheral $CD4^+CD25^+$ fraction (35). On the other hand, asbestos is a mineral silicate that contains magnesium, iron, and calcium, with a core of SiO_2 (36, 37). Thus, asbestos may affect human immunocompetent cells because silica can modify human immunity (32–35). In view of these facts, if we think about the medical complications of a population exposed to silica or asbestos, patients may exhibit a reduced antitumor immune function because of developing cancers possessing a long-term latent phase (20–50 years) after an initial exposure to asbestos (29–31).

Therefore, we previously investigated the effects of asbestos on NK cells, and reported impairment in the cytotoxicity and expression of NK cell–activating receptor NKp46 and a decrease in the phosphorylation of the extracellular signal–regulated kinase signaling molecule in NK cells exposed to asbestos (11, 12). We also studied the effects of asbestos in relation to $CD8^+$ cytotoxic T cells, and found impairment in the differentiation and proliferation of these cells, the details of which will be reported in the future.

In regard to $CD4^+$ T cells, we established an *in vitro* cell line model of low-level and continuous exposure to asbestos (17, 18). MT-2 cells (15, 16) were chosen and underwent an initial screening for growth inhibition by culturing with asbestos to detect sensitivity to asbestos-induced apoptosis, because cell lines derived from leukemia and lymphoma may already possess alterations in many cellular and molecular events due to transformation. Moreover, chrysotile was initially used to analyze the immunologic effects of asbestos, because this fiber is used widely throughout the world.

First, we reported that high-dose and transient exposure induced apoptosis in MT-2 cells, caused by the production of ROS, the activation of proapoptotic c-Jun N-terminal kinase and p38 signaling molecules in the mitogen-activated protein kinase pathway, and the activation of the mitochondrial apoptotic pathway, as shown in Figure 1 (18). These findings were also evident when CA including 2% fibrous anthophyllite was used for exposure, as described in alveolar epithelial and pleural mesothelial cells (5–10). Next, we established a subline exposed to long-term and low-level CB (17). This subline showed the acquisition of resistance to asbestos-induced apoptosis through an activation of Src-family kinases, the up-regulation of IL-10 production, the activation of STAT3, and the up-regulation of Bcl-2, as shown in Figure 1 (17). Furthermore, the expression of *Bcl-2* in $CD4^+$ T cells from patients with MM was significantly up-regulated compared with that in healthy donors (17). However, because we ran only one trial to establish the low-level and continuous exposure model, we cannot confirm whether the findings in this subline represent general responses.

Therefore, we established five other independent sublines involving long-term and low-level exposure to chrysotile, because the other altered molecules should be identified for a better understanding of the asbestos-induced reduction of antitumor immune function. As shown in Figures 2 and 7A, all

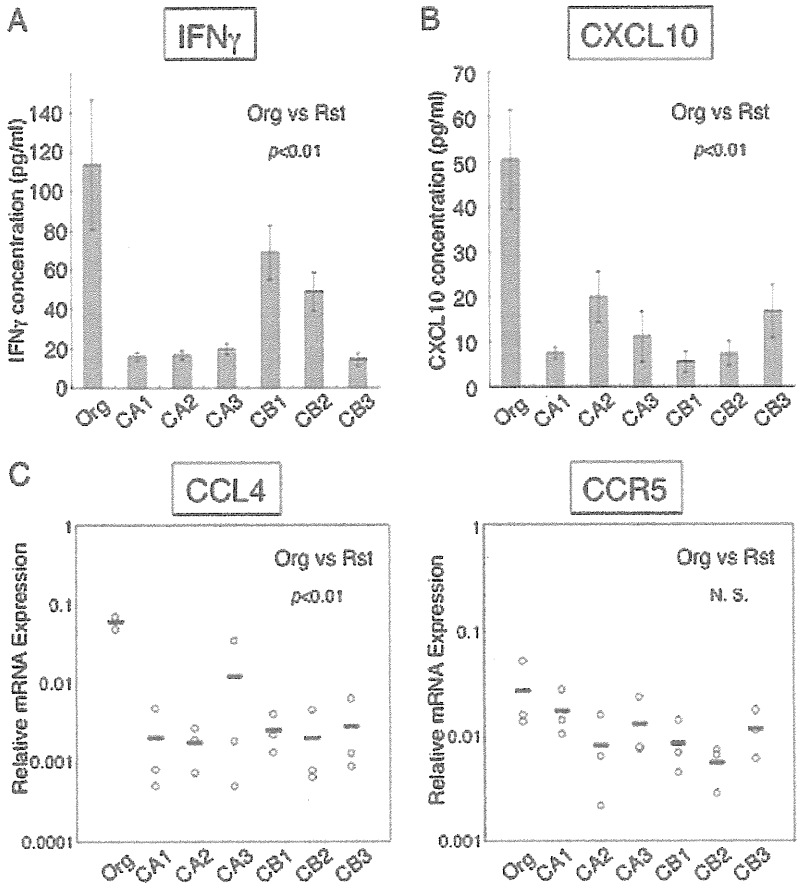

Figure 7. Continuous exposure to chrysotile decreases Th1-type cytokine IFN-γ and chemokine CXCL10/IP10 production in MT-2Rsts cells. (*A*, *B*) MT-2Org and MT-2Rsts cells were cultured for 72 hours. Culture supernatants were then collected and assessed for IFN-γ and CXCL10/IP10 production by ELISA. (*C*) The mRNA expressions of the Th1-type chemokine CCL4/MIP-1β and the receptor CCR5 were estimated using real-time RT-PCR. Results represent the mean ± SD of three independent experiments. *P* values were obtained using Dunnett's test. $^{*}P < 0.01$. $^{**}P < 0.05$.

six sublines, including the initial subline (CB1), exhibited a resistance to asbestos-induced apoptosis and a reduction of IFN-γ production, in a manner similar to that shown in previous studies (17). These findings indicate that the cellular and molecular alterations found in these sublines can be regarded as the universal immunologic effects of asbestos in T cells, although these findings should be confirmed using freshly isolated lymphocytes from both healthy donors and patients with MM exposed to asbestos.

An exhaustive analysis using DNA microarray, pathway, and network analyses identified the suppression of the Th1-type IFN-γ signaling pathway and CXCR3 expression. These alterations were confirmed by the decreased production of IFN-γ and decreased cell-surface expression of CXCR3 in all cell lines. IFN-γ is an antitumor cytokine, and it is used for the treatment of various cancers to enhance the antitumor activity of T cells, NK cells, and natural killer T cells (38, 39). In addition, the chemokine receptor CXCR3 is a G-protein–coupled seven-transmembrane receptor expressed on various lymphocytes, including T cells, B cells, and NK cells, and it binds to IFN-γ–inducible chemokines such as CXCL9/MIG, CXCL10/IP10, and CXCL11/I-TAC that recruit leukocytes to inflammatory sites such as tumors (40). In the case of $CD4^{+}$ T cells, CXCR3 is preferentially expressed on IFN-γ–producing Th1/effector T cells. Our previous study showed that original MT-2 cells exhibit a high-level production of inflammatory cytokine IFN-γ, TNF-α, and IL-6, whereas sublines produce an anti-inflammatory cytokine IL-10 at a high concentration (17), suggesting that the Th1/effector T-cell–like characteristics of MT-2Org cells may easily be suppressed by long-term and low-level exposures to chrysotile, although the mRNA expression of Th1-type CCR5 (41) was not inhibited significantly (Figure 7C). Moreover, all six sublines showed a down-regulation of Th1-type chemokine CXCL10/IP10 and CCL4/MIP-1β. Generally, both CXCL10/IP10 and CCL4/MIP-1β are secreted by activated T cells, and contribute to the attraction of Th1/effector T cells (41, 42). Therefore, the suppression of Th1-type molecules such as CXCR3, IFN-γ, CXCL10/IP10, and CCL4/MIP-1β in sublines continuously exposed to chrysotile can be considered evidence of asbestos-induced cellular and molecular alterations in immunocompetent cells. Exposure to asbestos seems to modify antitumor immune function and local (pulmonary) inflammatory reactions because of changes in the expression and production levels of cytokines, chemokines, and chemokine receptors in immune competent cells.

These findings may provide an explanation for the rapid progression of asbestos-related cancers, although further research is needed to confirm whether these alterations in cell-line models arise in freshly isolated human lymphocytes derived from healthy donors and patients with PP or MM.

Author Disclosure: None of the authors has a financial relationship with a commercial entity that has an interest in the subject of this manuscript.

Acknowledgments: We thank Tamayo Hatayama, Minako Kato, Naomi Miyahara, Shoko Yamamoto, Misao Kuroki, Keiko Kimura, Yoshiko Yamashita, and Tomoko Sueishi for technical assistance.

References

1. Pan XL, Day HW, Wang W, Beckett LA, Schenker MB. Residential proximity to naturally occurring asbestos and mesothelioma risk in California. *Am J Respir Crit Care Med* 2005;172:1019–1025.
2. Cugell DW, Kamp DW. Asbestos and the pleura: a review. *Chest* 2004; 125:1103–1117.
3. Miserocchi G, Sancini G, Mantegazza F, Chiappino G. Translocation pathways for inhaled asbestos fibers. *Environ Health* 2008;7:4.

4. Murayama T, Takahashi K, Natori Y, Kurumatani N. Estimation of future mortality from pleural malignant mesothelioma in Japan based on an age-cohort model. *Am J Ind Med* 2006;49:1–7.
5. Upadhyay D, Kamp DW. Asbestos-induced pulmonary toxicity: role of DNA damage and apoptosis. *Exp Biol Med (Maywood)* 2003;228: 650–659.
6. Panduri V, Surapureddi S, Soberanes S, Weitzman SA, Chandel N, Kamp DW. P53 mediates amosite asbestos–induced alveolar epithelial cell mitochondria–regulated apoptosis. *Am J Respir Cell Mol Biol* 2006;34:443–452.
7. Upadhyay D, Panduri V, Kamp DW. Fibroblast growth factor–10 prevents asbestos-induced alveolar epithelial cell apoptosis by a mitogen-activated protein kinase–dependent mechanism. *Am J Respir Cell Mol Biol* 2005;32:232–238.
8. Mossman BT. Introduction to serial reviews on the role of reactive oxygen and nitrogen species (ROS/RNS) in lung injury and diseases. *Free Radic Biol Med* 2003;34:1115–1116.
9. Kamp DW, Panduri V, Weitzman SA, Chandel N. Asbestos-induced alveolar epithelial cell apoptosis: role of mitochondrial dysfunction caused by iron-derived free radicals. *Mol Cell Biochem* 2002;234–235: 153–160.
10. Jiang L, Nagai H, Ohara H, Hara S, Tachibana M, Hirano S, Shinohara Y, Kohyama N, Akatsuka S, Toyokuni S. Characteristics and modifying factors of asbestos-induced oxidative DNA damage. *Cancer Sci* 2008;99:2142–2151.
11. Nishimura Y, Miura Y, Maeda M, Kumagai N, Murakami S, Hayashi H, Fukuoka K, Nakano T, Otsuki T. Impairment in cytotoxicity and expression of NK cell-activating receptors on human NK cells following exposure to asbestos fibers. *Int J Immunopathol Pharmacol* 2009;22:579–590.
12. Nishimura Y, Maeda M, Kumagai N, Hayashi H, Miura Y, Otsuki T. Decrease in phosphorylation of ERK following decreased expression of NK cell–activating receptors in human NK cell line exposed to asbestos. *Int J Immunopathol Pharmacol* 2009;22:879–888.
13. Ueki A, Yamaguchi M, Ueki H, Watanabe Y, Ohsawa G, Kinugawa K, Kawakami Y, Hyodoh F. Polyclonal human T-cell activation by silicate *in vitro*. *Immunology* 1994;82:332–335.
14. Aikoh T, Tomokuni A, Matsukii T, Hyodoh F, Ueki H, Otsuki T, Ueki A. Activation-induced cell death in human peripheral blood lymphocytes after stimulation with silicate *in vitro*. *Int J Oncol* 1998;12:1355–1359.
15. Miyoshi I, Kubonishi I, Yoshimoto S, Shiraishi Y. A T-cell line derived from normal human cord leukocytes by co-culturing with human leukemic T-cells. *Gann* 1981;72:978–981.
16. Miyoshi I, Kubonishi I, Yoshimoto S, Akagi T, Ohtsuki Y, Shiraishi Y, Nagata K, Hinuma Y. Type C virus particles in a cord T-cell line derived by co-cultivating normal human cord leukocytes and human leukaemic T cells. *Nature* 1981;294:770–771.
17. Miura Y, Nishimura Y, Katsuyama H, Maeda M, Hayashi H, Dong M, Hyodoh F, Tomita M, Matsuo Y, Uesaka A, *et al.* Involvement of IL-10 and Bcl-2 in resistance against an asbestos-induced apoptosis of T cells. *Apoptosis* 2006;11:1825–1835.
18. Hyodoh F, Takata-Tomokuni A, Miura Y, Sakaguchi H, Hatayama T, Hatada S, Katsuyama H, Matsuo Y, Otsuki T. Inhibitory effects of antioxidants on apoptosis of a human polyclonal T-cell line, MT-2, induced by an asbestos, chrysotile-A. *Scand J Immunol* 2005;61:442–448.
19. Maeda M, Miura Y, Nishimura Y, Murakami S, Hayashi H, Kumagai N, Hatayama T, Katoh M, Miyahara N, Yamamoto S, *et al.* Immunological changes in mesothelioma patients and their experimental detection. *Clin Med Insights Circ Respir Pulmon Med* 2008;2:11–17.
20. Nishimura Y, Miura Y, Maeda M, Hayashi H, Dong M, Katsuyama H, Tomita M, Hyodoh F, Kusaka M, Uesaka A, *et al.* Expression of the T cell receptor Vbeta repertoire in a human T cell resistant to asbestos-induced apoptosis and peripheral blood T cells from patients with silica and asbestos-related diseases. *Int J Immunopathol Pharmacol* 2006;19:795–805.
21. Kohyama N, Shinohara Y, Suzuki Y. Mineral phases and some reexamined characteristics of the International Union against Cancer standard asbestos samples. *Am J Ind Med* 1996;30:515–528.
22. Luster AD, Leder P. IP-10, a -C-X-C- chemokine, elicits a potent thymus-dependent antitumor response *in vivo*. *J Exp Med* 1993;178: 1057–1065.
23. Abraham JL. Recent advances in pneumoconiosis: the pathologist's role in etiologic diagnosis. *Monogr Pathol* 1978;19:96–137.
24. Vallyathan NV, Green FH, Craighead JE. Recent advances in the study of mineral pneumoconiosis. *Pathol Annu* 1980;15:77–104.
25. Begin R, Cantin A, Masse S. Recent advances in the pathogenesis and clinical assessment of mineral dust pneumoconioses: asbestosis, silicosis and coal pneumoconiosis. *Eur Respir J* 1989;2:988–1001.
26. Scheule RK, Holian A. Immunologic aspects of pneumoconiosis. *Exp Lung Res* 1991;17:661–685.
27. Uber CL, McReynolds RA. Immunotoxicology of silica. *Crit Rev Toxicol* 1982;10:303–319.
28. Steenland K, Goldsmith DF. Silica exposure and autoimmune diseases. *Am J Ind Med* 1995;28:603–608.
29. Kannerstein M, Churg J, McCaughey WT. Asbestos and mesothelioma: a review. *Pathol Annu* 1978;13:81–129.
30. Kannerstein M, Churg J, McCaughey E, Selikoff IJ. Pathogenic effects of asbestos. *Arch Pathol Lab Med* 1977;101:623–628.
31. Craighead JE, Mossman BT. The pathogenesis of asbestos-associated diseases. *N Engl J Med* 1982;306:1446–1455.
32. Otsuki T, Miura Y, Nishimura Y, Hyodoh F, Takata A, Kusaka M, Katsuyama H, Tomita M, Ueki A, Kishimoto T. Alterations of Fas and Fas-related molecules in patients with silicosis. *Exp Biol Med (Maywood)* 2006;231:522–533.
33. Otsuki T, Maeda M, Murakami S, Hayashi H, Miura Y, Kusaka M, Nakano T, Fukuoka K, Kishimoto T, Hyodoh F, *et al.* Immunological effects of silica and asbestos. *Cell Mol Immunol* 2007;4:261–268.
34. Wu P, Hyodoh F, Hatayama T, Sakaguchi H, Hatada S, Miura Y, Takata-Tomokuni A, Katsuyama H, Otsuki T. Induction of CD69 antigen expression in peripheral blood mononuclear cells on exposure to silica, but not by asbestos/chrysotile-A. *Immunol Lett* 2005;98:145–152.
35. Wu P, Miura Y, Hyodoh F, Nishimura Y, Hatayama T, Hatada S, Sakaguchi H, Kusaka M, Katsuyama H, Tomita M, *et al.* Reduced function of $CD4^{+}25^{+}$ regulatory T cell fraction in silicosis patients. *Int J Immunopathol Pharmacol* 2006;19:357–368.
36. Pooley FD. Mineralogy of asbestos: the physical and chemical properties of the dusts they form. *Semin Oncol* 1981;8:243–249.
37. Stephens M, Gibbs AR, Pooley FD, Wagner JC. Asbestos induced diffuse pleural fibrosis: pathology and mineralogy. *Thorax* 1987;42: 583–588.
38. Rudge G, Barrett SP, Scott B, van Driel IR. Infiltration of a mesothelioma by IFN-gamma–producing cells and tumor rejection after depletion of regulatory T cells. *J Immunol* 2007;178:4089–4096.
39. Miller CH, Maher SG, Young HA. Clinical use of interferon-gamma. *Ann N Y Acad Sci* 2009;1182:69–79.
40. Rotondi M, Chiovato L, Romagnani S, Serio M, Romagnani P. Role of chemokines in endocrine autoimmune diseases. *Endocr Rev* 2007;28: 492–520.
41. Luther SA, Cyster JG. Chemokines as regulators of T cell differentiation. *Nat Immunol* 2001;2:102–107.
42. Loetscher M, Loetscher P, Brass N, Meese E, Moser B. Lymphocyte-specific chemokine receptor CXCR3: regulation, chemokine binding and gene localization. *Eur J Immunol* 1998;28:3696–3705.

Published OnlineFirst October 21, 2011; DOI:10.1158/1078-0432.CCR-11-0868

Clinical Cancer Research

Early [^{18}F]Fluorodeoxyglucose Positron Emission Tomography at Two Days of Gefitinib Treatment Predicts Clinical Outcome in Patients with Adenocarcinoma of the Lung

Ryo Takahashi, Haruhiko Hirata, Isao Tachibana, et al.

Clin Cancer Res 2012;18:220-228. Published OnlineFirst October 21, 2011.

Published OnlineFirst October 21, 2011; DOI:10.1158/1078-0432.CCR-11-0868

Clinical Cancer Research

Imaging, Diagnosis, Prognosis

Early [^{18}F]Fluorodeoxyglucose Positron Emission Tomography at Two Days of Gefitinib Treatment Predicts Clinical Outcome in Patients with Adenocarcinoma of the Lung

Ryo Takahashi[1], Haruhiko Hirata[1], Isao Tachibana[1], Eku Shimosegawa[2], Atsuo Inoue[2], Izumi Nagatomo[1], Yoshito Takeda[1], Hiroshi Kida[1], Sho Goya[1], Takashi Kijima[1], Mitsuhiro Yoshida[1], Toru Kumagai[1], Atsushi Kumanogoh[1], Meinoshin Okumura[3], Jun Hatazawa[2], and Ichiro Kawase[4]

Abstract

Purpose: Positron emission tomography (PET) with [^{18}F]fluorodeoxyglucose (FDG) is increasingly used in early assessment of tumor response after chemotherapy. We investigated whether a change in [^{18}F]FDG uptake at 2 days of gefitinib treatment predicts outcome in patients with lung adenocarcinoma.

Experimental Design: Twenty patients were enrolled. [^{18}F]FDG-PET/computed tomographic (CT) scan was carried out before and 2 days after gefitinib treatment. Maximum standardized uptake values (SUV) were measured, and post-gefitinib percentage changes in SUV were calculated. Early metabolic response (SUV decline < −25%) was compared with morphologic response evaluated by CT scan and with progression-free survival (PFS).

Results: At 2 days of gefitinib treatment, 10 patients (50%) showed metabolic response, 8 had metabolic stable disease, and 2 had progressive metabolic disease. Percentage changes of SUV at 2 days were correlated with those of tumor size in CT at 1 month ($R^2 = 0.496$; $P = 0.0008$). *EGFR* gene was assessable in 15 patients, and of 12 patients with *EGFR* mutations, 8 showed metabolic response at 2 days and 6 showed morphologic response at 1 month. None of 3 patients with wild-type *EGFR* showed metabolic or morphologic response. Metabolic response at 2 days was not statistically associated with PFS ($P = 0.095$), but when a cutoff value of −20% in SUV decline was used, metabolic responders had longer PFS ($P < 0.0001$).

Conclusion: Early assessment of [^{18}F]FDG tumor uptake with PET at 2 days of gefitinib treatment could be useful to predict clinical outcome earlier than conventional CT evaluation in patients with lung adenocarcinoma. *Clin Cancer Res; 18(1); 220–8. ©2011 AACR.*

Introduction

Treatment of non–small cell lung cancer (NSCLC) has made remarkable progress in the last decade; the epidermal growth factor receptor (EGFR), which is expressed in more than 60% of patients with metastatic NSCLC and correlates with poor prognosis (1), has emerged as an important molecular target for advanced or recurrent NSCLC. Reversible EGFR tyrosine kinase inhibitors (TKI), gefitinib and erlotinib, were found to have antitumor activities in second- or third-line therapy (2–4). Objective responses with these agents were limited to a subpopulation of patients, which included never-smokers, women, East Asians, and patients with adenocarcinoma histology (4, 5). It was later shown that most of these responders harbor specific mutations or increased copy number in the gene encoding EGFR that enhances tyrosine kinase activity (6, 7). Indeed, gefitinib as first-line and single-agent therapy improved progression-free survival (PFS) of patients with NSCLC with the *EGFR* mutations when compared with standard chemotherapy (8–10). Although these genetic markers may be used to predict therapeutic response, they do not guarantee successful treatment as a portion of marker-positive patients did not respond to the EGFR TKIs, whereas a portion of marker-negative patients did respond (11). Moreover, a secondary mutation in the *EGFR* gene or amplification of *c-Met* negates the sensitizing effect, leading to acquired

Authors' Affiliations: Departments of [1]Respiratory Medicine, Allergy and Rheumatic Diseases, [2]Nuclear Medicine, and [3]General Thoracic Surgery, Osaka University Graduate School of Medicine; and [4]Osaka Prefectural Medical Center for Respiratory and Allergic Diseases, Osaka, Japan

Note: Supplementary data for this article are available at Clinical Cancer Research Online (http://clincancerres.aacrjournals.org/).

R. Takahashi and H. Hirata contributed equally to the work as the first authors.

Corresponding Author: Isao Tachibana, Department of Respiratory Medicine, Allergy and Rheumatic Diseases, Osaka University Graduate School of Medicine, 2-2 Yamada-oka, Suita, Osaka 565-0871, Japan. Phone: 81-6-6879-3833; Fax: 81-6-6879-3839; E-mail: itachi02@imed3.med.osaka-u.ac.jp

doi: 10.1158/1078-0432.CCR-11-0868

Published OnlineFirst October 21, 2011; DOI:10.1158/1078-0432.CCR-11-0868

Translational Relevance

It remains difficult to accurately predict clinical benefit of gefitinib in patients with non–small cell lung cancer (NSCLC). A recent basic study using a mouse model has shown that gefitinib induces a decrease of fluorodeoxyglucose (FDG) uptake within 48 hours in sensitive NSCLC tumors. We conducted a pilot study to validate the use of early FDG-positron emission tomography (PET) in clinical settings. Assessment of FDG uptake only after 2 days of gefitinib treatment was able to predict tumor response and progression-free survival. This early assessment could help to identify patients who will benefit from gefitinib therapy while allowing for rapid initiation of alternative strategies and minimizing critical adverse effects such as interstitial lung disease when gefitinib is ineffective.

resistance to the EGFR TKIs (12). Thus, it appears difficult to predict clinical benefit accurately only with these genetic biomarkers.

Positron emission tomography (PET) with [^{18}F]fluorodeoxyglucose (FDG) plays a role in the diagnosis and staging of lung cancer. It is based on high glucose metabolism in tumor cells that have an increased level of glucose transport protein expression and hexokinase activity. In addition to diagnosis and staging, [^{18}F]FDG-PET is increasingly used to assess tumor response and to predict outcome. A decrease in FDG uptake in sensitive tumor cells can be detected earlier than structural changes occur (13). This is the case especially in tumors treated with molecularly targeted drugs rather than with cytotoxic agents. In gastrointestinal stromal tumors (GIST), FDG-PET has been shown to be highly sensitive in detecting early response to imatinib mesylate, a small molecule that inhibits c-KIT. Decreases in FDG uptake were observed after 1 week of treatment, whereas volume responses evaluated on computed tomographic (CT) scan were small and developed more slowly (14, 15). In NSCLC, it has remained unknown that how EGFR TKIs downregulate FDG uptake after initiation of treatment in sensitive tumors. Recently, using a mouse xenograft model, Su and colleagues showed rapid decreases of tumor FDG uptake in sensitive xenografts within 48 hours of gefitinib treatment (16). They also found a decline in FDG uptake 24 to 48 hours before inhibition of proliferation and induction of apoptosis in a gefitinib-sensitive NSCLC cell line. A more recent preliminary study, which evaluated [^{18}F]FDG-PET in 5 patients with advanced NSCLC treated with gefitinib, suggested that FDG-PET may be able to predict the response. Patients exhibiting a partial response on CT evaluation already showed a mean of 61% decrease in FDG uptake at 2 days of therapy (17). Thus, further prospective studies are needed to confirm that [^{18}F]FDG-PET provides an early sensitive marker of the effectiveness of gefitinib in patients with NSCLC.

In the present study, we prospectively evaluated FDG-PET only after 2 days of gefitinib treatment in patients with lung adenocarcinoma to predict response and outcome. We used a combined PET/CT scan to provide correct anatomic registration of PET data.

Materials and Methods

Patients

Twenty patients with lung adenocarcinoma who received gefitinib treatment were enrolled from November 2007 to November 2009. Diagnosis was made either histologically or cytologically. Gefitinib at a dose of 250 mg once a day was administered orally 30 minutes after breakfast as the first EGFR tyrosine kinase inhibition therapy, until disease progression, unacceptable toxicity, or patient refusal. Eligibility criteria included an age of 20 years or more, unresectable stage or relapse after surgery, measurable disease, and Eastern Cooperative Oncology Group (ECOG) performance status of 0 to 2. The study protocol was approved by the Institutional Review Board of Osaka University Hospital, Osaka, Japan, and written informed consent was obtained from all patients.

EGFR mutation analysis

Mutation analysis of *EGFR* in exons 18, 19, 20, and 21 was conducted using biopsy specimens obtained at diagnosis. Genomic DNA was extracted and analyzed by peptide nucleic acid–locked nucleic acid PCR (PNA-LNA PCR) cramp method manufactured in Mitsubishi Chemical Medience Co., as previously described (18).

FDG-PET/CT

[^{18}F]FDG-PET/CT was conducted before (at baseline), 2 days, and 1 month after gefitinib administration using a GEMINI GXL scanner (Philips Medical Systems). Baseline scan was done within 14 days prior to the treatment. All patients were fasted for at least 4 hours before scanning. Their serum glucose levels were less than 150 mg/dL before FDG injection. One hour after the injection of 3.7 MBq/kg [^{18}F]FDG, patients were scanned from the head to the thigh. We calculated accurate [^{18}F]FDG uptake time for each patient and confirmed that there was no significant difference between any metabolic responders and nonresponders. After a 50-mAs low-dose CT scan for attenuation correction, emission scan was obtained in a 3-demensional acquisition mode at 11 to 12 bed positions with 2 min/bed speed. In-plane and axial field of view of the scanner were 576 mm and 180 mm, respectively. In-plane spatial resolution was 6.31 mm full width at half maximum (FWHM) at the center with 144 × 144 pixel size (4 × 4 × 4 mm^3/pixel). Images were reconstructed by line-of-response row-action maximum likelihood algorithm (LOR-RAMLA) method. After acquisition of the PET images, a diagnostic chest CT was conducted by a 16-row multidetector scanner in a helical mode with 120 kV of the tube voltage and 200 mAs of the effective tube current. CT gantry rotation time was 0.5 seconds with an axial field of view of 600 mm,

Published OnlineFirst October 21, 2011; DOI:10.1158/1078-0432.CCR-11-0868

producing 5-mm thick slices with a 512 × 512 matrix. Regions of interest were placed over the highest accumulation area, corresponding to tumor sites on the PET images. The maximal standardized uptake value (SUV) was determined as previously described (19).

Response assessment and follow-up

Among measurable lesions according to the Response Evaluation Criteria in Solid Tumors version 1.0 (RECIST 1.0; ref. 20) in fused mode of dual modality PET/CT, up to 5 lesions in order of [^{18}F]FDG uptake level were defined as target lesion on the baseline scan. [^{18}F]FDG uptake was evaluated as the SUV of the target lesions (21). The lowest SUV of target lesions was 1.6, which was still higher than the background (Table 1). On PET/CT at 2 days and 1 month of gefitinib administration, percentage changes in the sum of these SUVs of the target metabolic lesions were determined on the basis of the baseline scan, and time point metabolic response was defined according to the recommendations of the European Organization for Research and Treatment of Cancer (EORTC) PET study group (22). Complete metabolic response (CMR) was achieved when SUVs of all lesions were decreased to uptake equivalent to background. Partial metabolic response (PMR) was defined as percentage change of the sum of SUVs (ΔSUV%) < −25%, stable metabolic disease (SMD) was −25% ≤ ΔSUV% < +25%, and progressive metabolic disease (PMD) was defined as +25% ≤ ΔSUV% or when the extent of [^{18}F]FDG increased greater than 20% in the longest dimension or when new [^{18}F]FDG uptake appeared in metastatic lesions. In analysis of PFS, a cutoff value of −20%, instead of −25%, was also used to separate responders from nonresponders. Changes in tumor size of the same target lesions as [^{18}F]FDG uptake analysis and nontarget lesions were quantified on CT images from PET/CT data at 1 month by 2 of the authors blinded to the PET data, and time point overall response was classified according to RECIST 1.0. Percentage changes in the sum of the longest dimension (ΔCTsize%) of the target lesions were also determined and compared with ΔSUV%. On CT images at 2 days of gefitinib administration, all patients were with stable disease. Chest CT or radiograph was repeated every 4 weeks until disease progression, which was determined by RECIST 1.0. The overall responses classified at 1 month were not confirmed by the repeat assessments in this study.

Table 1. Patient characteristics at baseline

Characteristic	*N*
Total no. of patients	20
Sex	
Male	5
Female	15
Age, y	
Median	69
Range	58–83
ECOG performance status	
0	10
1	10
Smoking history	
Never	15
Ever	5
Clinical stage	
IIIA	2
IIIB	3
IV	15
No. of prior chemotherapy	
0	10
1	6
2	2
3	1
4	1
EGFR mutation status	
Exon 19	6
Exon 21	5
Exon 18	1
Wild-type	3
Not determined	1
Not tested	4
Baseline study	
No. of target lesions	
Median	2.5
Range	1–5
SUV of target lesions	
Median	5.9
Range	1.6–13.0
Size of target lesions, cm	
Median	2.0
Range	1.2–7.7

Statistical analysis

Data were analyzed using JMP statistical discovery software version 8.0.2 (SAS Institute). Correlation between ΔSUV% at 2 days and ΔCTsize% at 1 month was evaluated by Fisher ANOVA. Agreement between the EORTC recommendations–based metabolic response at 2 days and RECIST-based morphologic overall response at 1 month was evaluated using kappa statistic (23). PFS was measured from the first administration of gefitinib to documented progression or death of any cause. Overall survival (OS) was from the first administration of gefitinib to death of any cause. PFS and OS were estimated using the Kaplan–Meier method and compared by the 2-sided log-rank test (24). HRs were calculated using the Cox proportional hazards model. In multivariate Cox model analysis, metabolic response at 2 days and morphologic response at 1 month, significance of which was $P < 0.15$ in univariate analysis, were chosen as variable in addition to smoking history, which was previously shown to be a prognostic factor for patients with gefitinib-treated NSCLC (5). *EGFR* mutation status was not included because it was not determined or tested in 5 patients, and the number of patients with wild-type *EGFR* was only 3.

Published OnlineFirst October 21, 2011; DOI:10.1158/1078-0432.CCR-11-0868

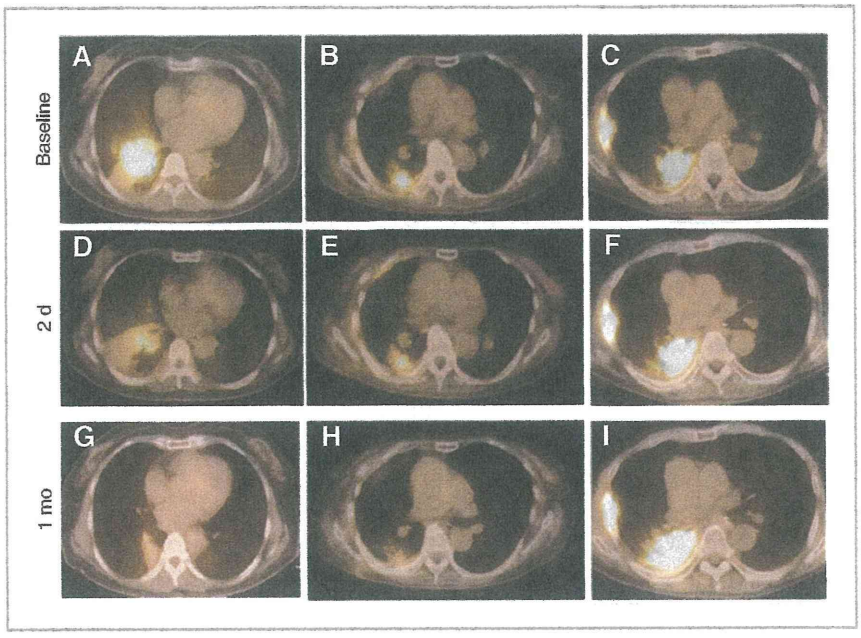

Figure 1. Pre- and posttreatment images of FDG-PET/CT scans of a 67-year-old female (A, D, and G) and a 75-year-old female (B, E, and H), who achieved partial response at 1 month (G and H, respectively), and an 81-year-old male (C, F, and I), who had progressive disease at 1 month (I) as assessed by RECIST 1.0. The first 2 patients already showed partial metabolic response at 2 days (D and E), and the third patient was assessed with progressive metabolic disease at 2 days (F).

Results

Patient characteristics

A total of 20 patients (15 females and 5 males) were enrolled in this study, underwent PET/CT for baseline assessment, and received gefitinib treatment. Nineteen were patients with adenocarcinoma and one with adenosquamous carcinoma. Fifteen patients (75%) had clinical stage IV disease. Five patients at clinical stage III were not treated with surgery or radiation due to the presence of malignant pleural effusion and complicating diseases. Ten were previously untreated and 10 had been treated with 1 to 4 chemotherapy regimens. Detailed patient characteristics are shown in Table 1. Median time between the baseline PET/CT and the start of gefitinib treatment was 4 days (range, 0–13 days), and no chemotherapy was administered during this period. A 77-year-old male patient did not complete PET/CT at 1 month because ground-glass opacity appeared on chest radiograph and gefitinib administration was discontinued at 6 days of treatment; this patient was excluded from later assessment. In all the other patients, gefitinib was continued to documented disease progression, and none of them received additional treatment without documented progression. Overall, early response at 2 days was assessed in 20 patients, and late response assessment at 1 month and PFS analysis were conducted in 19 patients.

Comparative analysis of metabolic and morphologic responses

Metabolic responses could be detected only at 2 days of treatment, when morphologic responses were still unrecognizable. Representative PET/CT images of responders and nonresponders during gefitinib treatment were shown in Fig. 1. Median percentage change of the sum of SUVs (ΔSUV%) of target lesions was −23%. Sixteen patients experienced ΔSUV% reduction ranging from −2% to −52% (Fig. 2A). No patient achieved a complete metabolic response (SUVs of all lesions equivalent to background) and 10 (50%) patients achieved a partial metabolic response (ΔSUV% < −25%). Four patients experienced an increase of ΔSUV% ranging from +6% to +36% and 2 of these were assessed with progressive metabolic disease (+25% ≤ ΔSUV%). These changes of target lesions in SUV at 2 days of treatment were compared with those in tumor size (ΔCTsize%) at 1 month of treatment, which was quantified on CT images, and there was a strong correlation ($R^2 = 0.496$; $P = 0.0008$) as shown in Fig. 2B. There was also a moderate agreement ($\kappa = 0.566$) between metabolic responses at 2 days based on the EORTC recommendations and morphologic overall responses at 1 month according to RECIST 1.0 (Fig. 2C). Of 10 metabolic responders at 2 days, 8 patients were morphologic responders and 2 were with stable disease by RECIST 1.0 at 1 month. Of 7 patients with stable metabolic disease (−25% ≤ ΔSUV% < +25%) at 2 days, 5 patients were assessed with morphologically stable disease and 2 had progressive disease by RECIST 1.0 at 1 month. Median PFS of patients with partial metabolic response, stable metabolic disease, and progressive metabolic disease was 290, 48, and 39 days, respectively. Median PFS of patients with morphologic partial response, stable disease, and progressive disease was 267, 100, and 29 days, respectively.

EGFR mutation

Biopsy samples from 5 patients were not suitable for molecular analysis. Mutation of *EGFR* gene was assessable in 15 patients and 12 were *EGFR* mutation positive:

Published OnlineFirst October 21, 2011; DOI:10.1158/1078-0432.CCR-11-0868

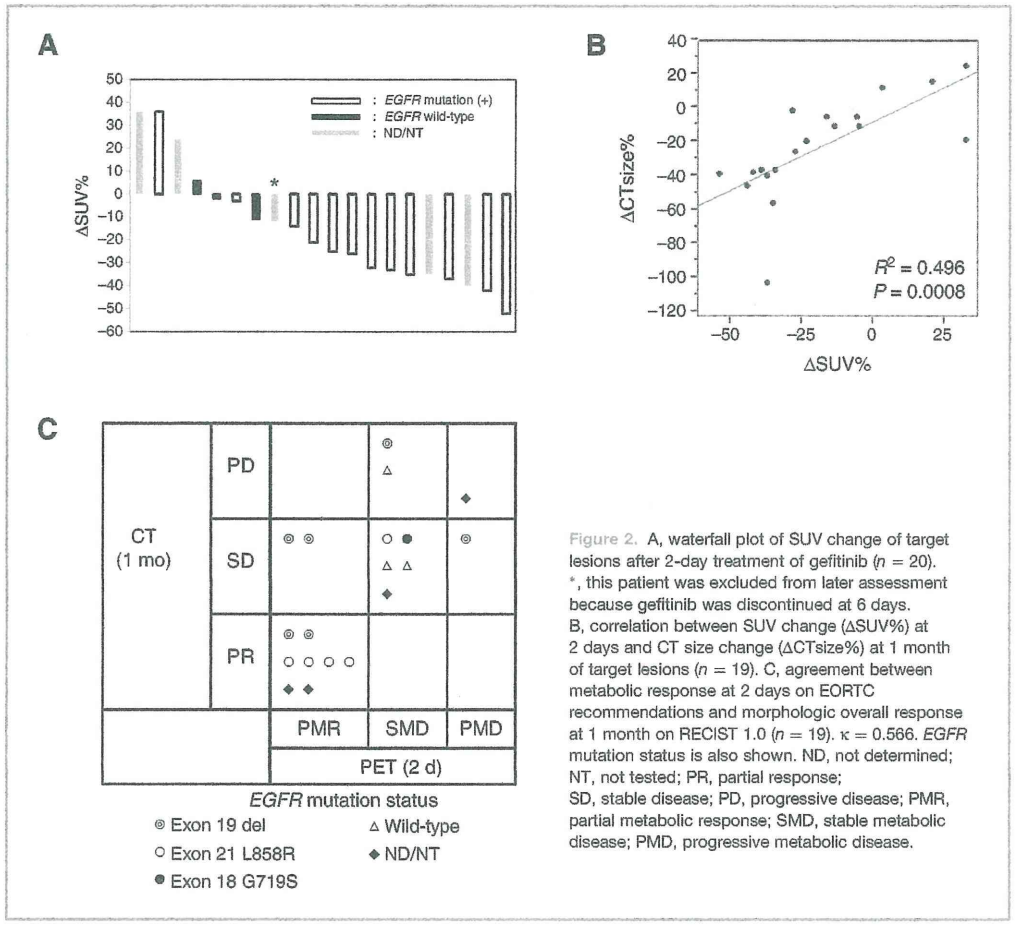

Figure 2. A, waterfall plot of SUV change of target lesions after 2-day treatment of gefitinib ($n = 20$). *, this patient was excluded from later assessment because gefitinib was discontinued at 6 days. B, correlation between SUV change (ΔSUV%) at 2 days and CT size change (ΔCTsize%) at 1 month of target lesions ($n = 19$). C, agreement between metabolic response at 2 days on EORTC recommendations and morphologic overall response at 1 month on RECIST 1.0 ($n = 19$). $\kappa = 0.566$. *EGFR* mutation status is also shown. ND, not determined; NT, not tested; PR, partial response; SD, stable disease; PD, progressive disease; PMR, partial metabolic response; SMD, stable metabolic disease; PMD, progressive metabolic disease.

6 patients had an exon 19 deletion, 5 patients had an exon 21 L858R mutation, and one had an exon 18 G719S mutation. Median ΔSUV% changes of target lesions in patients with mutated *EGFR* and wild-type *EGFR* were −29% and −2%, respectively (Fig. 2A). Of 12 patients with activating *EGFR* mutations, 8 (67%) were metabolic responders and 3 were with stable metabolic disease at 2 days, whereas 6 (50%) were morphologic responders and 5 were morphologically with stable disease at 1 month (Fig. 2C). Conversely, of 8 *EGFR* gene-assessable metabolic responders at 2 days, all had the activating mutations and 6 were assessed as morphologic responders at 1 month. Of 6 *EGFR* gene-assessable morphologic responders at 1 month, all had the mutations and were assessed as metabolic responders at 2 days. An 83-year-old female patient with an exon 19 deletion was assessed as having progressive metabolic disease while being with morphologically stable disease. During follow-up, this patient suffered from a relapse at 48 days. Another 79-year-old female patient with an exon 19 deletion was with stable metabolic disease at 2 days but assessed as having progressive disease because a new lesion appeared on PET/CT images at 1 month. All of 3 patients with wild-type *EGFR* were assessed with metabolically stable disease at 2 days. Two of these were assessed with morphologically stable disease and one had progressive disease at 1 month (Fig. 2C).

PFS according to metabolic and morphologic responses

When a cutoff value of −25% in ΔSUV% was used between metabolic responders and nonresponders, PFS did not significantly correlate with metabolic response at 2 days. Median PFS of the responders and nonresponders was 290 days and 48 days, respectively (log-rank $P = 0.095$; Fig. 3A). This was attributable to a 58-year-old male nonresponder with an L858R mutation who was assessed with 21% decrease of ΔSUV% and experienced the longest PFS of 680 days. When a cutoff value of −20%, which was still within the extent recommended by EORTC (22), was used, this patient was included in responders, and 2-day metabolic responders had significantly prolonged PFS compared with metabolic nonresponders (median, 296 vs. 42 days; $P < 0.0001$; Fig. 3B). When metabolic response was evaluated at 1 month, PFS was also significantly longer in

Published OnlineFirst October 21, 2011; DOI:10.1158/1078-0432.CCR-11-0868

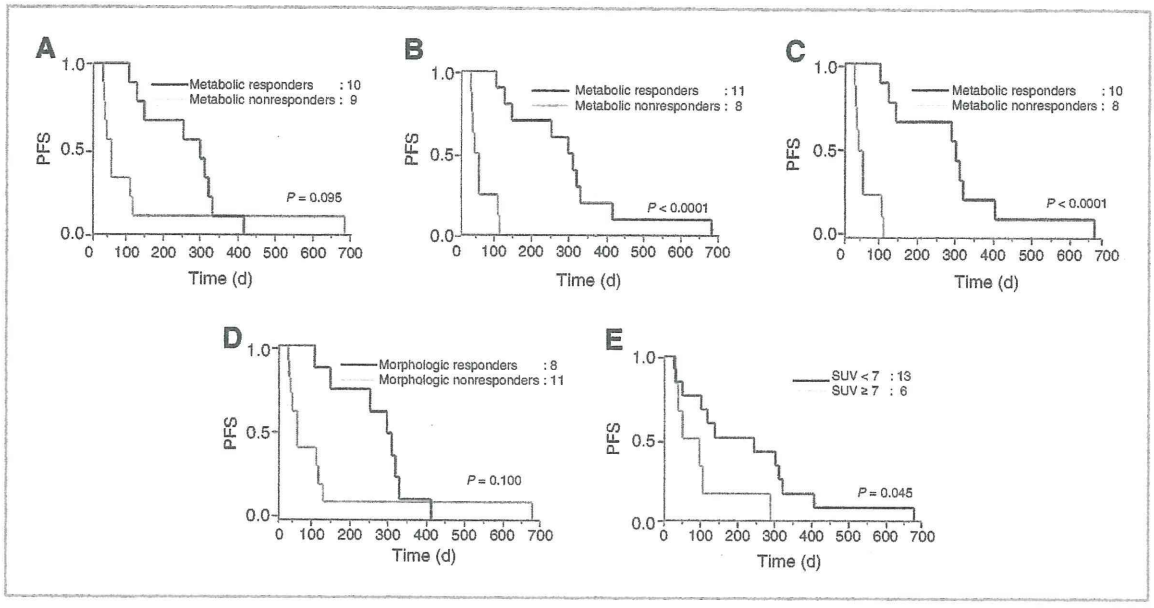

Figure 3. A, PFS of metabolic responders (ΔSUV% < −25%) and nonresponders (ΔSUV% ≥ −25%) at 2 days. B, PFS of metabolic responders (ΔSUV% < −20%) and nonresponders (ΔSUV% ≥ −20%) at 2 days. C, PFS of metabolic responders (ΔSUV% < −25%) and nonresponders (ΔSUV% ≥ −25%) at 1 month. One patient did not have an FDG-PET scan at 1 month, without missing a CT scan. D, PFS of morphologic responders and nonresponders at 1 month. E, PFS according to a single PET activity at 2 days (SUV < 7, black; SUV ≥ 7, gray). *P* values were obtained using the log-rank test.

responders than in nonresponders even with the cutoff value of −25% (median, 302 vs. 42 days; $P < 0.0001$; Fig. 3C). Meanwhile, PFS did not correlate with morphologic response based on RECIST 1.0 even at 1 month of treatment (median, 296 vs. 48 days; $P = 0.100$; Fig. 3D) because the patient with the longest PFS of 680 days was assessed with stable disease. When this patient was excluded, 1-month morphologic response became significantly correlated with PFS ($P = 0.0003$).

In the clinical settings, SUV at baseline PET might be influenced by previous chemotherapy. Therefore, we also investigated whether an early metabolic assessment with a single post-gefitinib PET/CT scan would provide any useful prognostic information. We defined an SUV threshold of 7, which was the nearest integer to the average SUV of the hottest target lesions in PET at 2 days, to separate responders (i.e., SUV < 7) from poor responders (SUV ≥ 7). There was a significant association between post-gefitinib FDG uptake and PFS (median, 244 days with SUV < 7 vs. 71 days with SUV ≥ 7; $P = 0.045$; Fig. 3E). Meanwhile, SUV in baseline PET studies was not predictive of PFS (median, 117 days with SUV < 10 vs. 93 days with SUV ≥ 10; $P = 0.611$).

In univariate analysis using the Cox hazards model, metabolic response using a cutoff value of −20% of ΔSUV% at 2 days was the only predictive factor of PFS (HR = 0.04; $P < 0.0001$), other than *EGFR* mutation status (Table 2).

Table 2. Univariate analysis of predictive factors for PFS

	Analysis		
Predictive factor	***n***	**HR (95% CI)**	***P***
Age (≥70 y)	19	1.69 (0.60–4.58)	0.310
Sex (female)	19	1.19 (0.37–5.29)	0.789
Smoking history (never)	19	1.22 (0.39–5.46)	0.747
Metabolic response at 2 d[a] (yes)	19	0.04 (0.002–0.23)	<0.0001
Morphologic response at 1 mo (yes)	19	0.44 (0.16–1.20)	0.109
EGFR mutation (yes)	15	0.17 (0.03–0.92)	0.041

[a]A cutoff value of −20% in SUV decline was used.

Published OnlineFirst October 21, 2011; DOI:10.1158/1078-0432.CCR-11-0868

In multivariate analysis including metabolic response at 2 days, morphologic response at 1 month, and smoking history, metabolic response at 2 days was the only statistically significant factor ($P = 0.0007$).

OS according to metabolic and morphologic responses

OS did not differ significantly between any metabolic responders and nonresponders and between the morphologic responders and nonresponders (Supplementary Fig. S1), although there was a trend for longer survival in metabolic responders who showed post-gefitinib SUV < 7 at 2 days ($P = 0.066$; Supplementary Fig. S1E).

Discussion

It has been evident that EGFR TKIs, gefitinib and erlotinib, induce dramatic responses in a subpopulation of patients with adenocarcinoma. Although the presence of somatic mutations in the *EGFR* gene is considered to be the best predictor of response to these TKIs (9, 10, 25, 26), its efficacy as biomarker is not satisfactory due to technical problems on biopsy, secondary mutation acquiring the resistance to the EGFR TKIs, and recent data showing response of patients with wild-type *EGFR* to erlotinib (27). Thus, an alternative approach optimizing clinical outcome of EGFR TKI therapy is necessary to accurately select patients who will benefit from the therapy and to avoid critical adverse effects such as interstitial lung disease (28).

Early response to therapy assessed by [^{18}F]FDG-PET has been increasingly established as a prognostic biomarker in various malignancies (13). In NSCLC, two studies have just been published to show that early [^{18}F]FDG-PET evaluation can predict PFS and OS in patients treated with erlotinib (29, 30). Another recent study reported that early [^{18}F]FDG-PET predicted histopathologic response in patients with NSCLC treated with erlotinib as neoadjuvant therapy (31). Metabolic tumor responses were assessed 1 to 8 weeks after the start of erlotinib treatment in these studies. Meanwhile, Su and colleagues showed that gefitinib treatment induced rapid decreases of FDG uptake within 48 hours in sensitive tumors using a mouse model, providing a rationale for earlier assessment in clinical settings (16). In these sensitive tumors, glucose transporters rapidly translocated from the plasma membrane to the cytosol, and reduction of hexokinase activity was observed prior to changes in cell-cycle distribution, thymidine uptake, and apoptosis. Such changes were not found in an early decline of FDG uptake in response to conventional cytotoxic chemotherapy (32). A more recent study preliminarily analyzed 5 patients with advanced NSCLC and reported that, only 2 days after initiation of gefitinib therapy, SUV decreased by a mean of 61% in patients who showed partial response by conventional CT evaluation 4 weeks later (17).

Consistent with these studies, SUV decreased by up to a maximum of 52% at 2 days in the present prospective study, and we observed a strong correlation between changes in SUV at 2 days and those in tumor size at 1 month. There was also a moderate agreement between metabolic responses at 2 days based on the EORTC recommendations and morphologic responses at 1 month according to RECIST 1.0. Moreover, metabolic response at 2 days could be a predictor of prolonged PFS when a cutoff value of −20% in SUV decline was used. The cutoff value of −25%, which was used in several other studies (33–35) but did not reach statistical significance in the present study, might be too large for the evaluation only after 2 days and for the sample size as small as 20. A single PET study at 2 days might also provide prognostic information. Patients with favorable response with lower post-gefitinib SUVs (SUV < 7) revealed longer PFS than poorly responding patients with higher SUVs (SUV ≥ 7), although significance was weak. There was a trend for an association between morphologic response at 1 month and improved PFS but it did not reach statistical significance, due to the presence of an *EGFR* mutation-positive patient showing stable disease but with a long PFS. In terms of OS, there was not significant difference, probably due to the small sample size and because OS is influenced by the second-line or later treatment. Together, although our study was a single-centered with a small number of patients, we propose that assessment of FDG uptake at 2 days could be a superior predictor of post-gefitinib outcome to conventional CT evaluation in its accuracy and rapidity.

Of 12 patients with activating *EGFR* mutations, 10 (83%) showed partial response or were with stable disease both in FDG-PET at 2 days and CT evaluation at 1 month. Thus, mutated *EGFR* is a good biomarker for response to gefitinib, as previously reported (6). Exceptionally, an 83-year-old female patient with exon 19 deletion had progressive metabolic disease at 2 days while being with morphologically stable disease at 1 month. She had a PFS of 48 days and this was relatively short for morphologically stable disease, the median PFS of which was 100 days. Another 79-year-old female patient with exon 19 deletion was with stable metabolic disease at 2 days while having morphologically progressive disease at 1 month. Her PFS was 30 days and relatively short for stable metabolic disease, the median PFS of which was 48 days. Thus, there was still inconsistency among *EGFR* mutations, early FDG-PET evaluation, or conventional CT evaluation, and larger prospective studies will be needed to clarify which is the best predictor of survival. Meanwhile, although it appears reasonable that none of 3 patients with wild-type *EGFR* showed metabolic or morphologic response, the number of patients is too small to discuss more about wild-type *EGFR*.

Interstitial lung disease is the most severe adverse effect, which occurs in approximately 1% of EGFR TKI–treated patients worldwide. Onset of symptoms may begin only after 2 days of gefitinib therapy. Median onset was 24 days in Japan and 42 days in United States, and about 1 of 3 of the cases were fatal (28). It has been suggested that [^{18}F]FDG-PET may help to evaluate interstitial lung disease. Positive FDG uptake was observed in 86% of patients with idiopathic pulmonary fibrosis and correlated with disease

Published OnlineFirst October 21, 2011; DOI:10.1158/1078-0432.CCR-11-0868

activity (36). In the present study, a 77-year-old male patient showed ground-glass opacity suggestive of interstitial infiltrate on chest radiograph, and gefitinib was discontinued at 6 days of treatment. At 2 days of treatment, his PET images did not show any positive uptake in lung parenchyma, and later on a CT scan, this infiltrate was rather considered a secondary change associated with obstructive bronchus. No other patient presented with interstitial infiltrate on chest radiograph. Thus, we could not determine at the moment whether [^{18}F]FDG-PET can early detect gefitinib-induced lung damage.

In summary, early response assessment by FDG-PET could help to identify patients with lung adenocarcinoma who will benefit from gefitinib treatment. The present study showed promising data suggesting that clinical outcome can be predicted only after 2 days of the treatment. This early assessment may allow for rapid initiation of alternative strategies and minimize critical adverse effects such as interstitial lung disease when gefitinib is ineffective. The main limitation is the small sample size, and validation with prospective studies in a larger patient population is warranted.

Disclosure of Potential Conflicts of Interest

No potential conflicts of interest were disclosed.

Acknowledgments

The authors thank Y. Habe for secretarial assistance.

Grant Support

The work was supported by the grand-in-aid for community health and medical care from the Osaka University Medical School Alumni and the award from the Osaka Cancer Association. This trial is registered at www.umin.ac.jp/ctr/index/htm as UMIN000003621.

The costs of publication of this article were defrayed in part by the payment of page charges. This article must therefore be hereby marked *advertisement* in accordance with 18 U.S.C. Section 1734 solely to indicate this fact.

Received April 14, 2011; revised October 6, 2011; accepted October 9, 2011; published OnlineFirst October 21, 2011.

References

1. Sharma SV, Bell DW, Settleman J, Haber DA. Epidermal growth factor receptor mutations in lung cancer. Nat Rev Cancer 2007;7:169–81.
2. Fukuoka M, Yano S, Giaccone G, Tamura T, Nakagawa K, Douillard JY, et al. Multi-institutional randomized phase II trial of gefitinib for previously treated patients with advanced non-small-cell lung cancer (The IDEAL 1 Trial) [corrected]. J Clin Oncol 2003;21:2237–46.
3. Kris MG, Natale RB, Herbst RS, Lynch TJ Jr, Prager D, Belani CP, et al. Efficacy of gefitinib, an inhibitor of the epidermal growth factor receptor tyrosine kinase, in symptomatic patients with non-small cell lung cancer: a randomized trial. JAMA 2003;290:2149–58.
4. Shepherd FA, Rodrigues Pereira J, Ciuleanu T, Tan EH, Hirsh V, Thongprasert S, et al. Erlotinib in previously treated non-small-cell lung cancer. N Engl J Med 2005;353:123–32.
5. Thatcher N, Chang A, Parikh P, Rodrigues Pereira J, Ciuleanu T, von Pawel J, et al. Gefitinib plus best supportive care in previously treated patients with refractory advanced non-small-cell lung cancer: results from a randomised, placebo-controlled, multicentre study (Iressa Survival Evaluation in Lung Cancer). Lancet 2005;366:1527–37.
6. Gazdar AF. Activating and resistance mutations of EGFR in non-small-cell lung cancer: role in clinical response to EGFR tyrosine kinase inhibitors. Oncogene 2009;28 Suppl 1:S24–31.
7. Hirsch FR, Varella-Garcia M, Cappuzzo F. Predictive value of EGFR and HER2 overexpression in advanced non-small-cell lung cancer. Oncogene 2009;28 Suppl 1:S32–7.
8. Mok TS, Wu YL, Thongprasert S, Yang CH, Chu DT, Saijo N, et al. Gefitinib or carboplatin-paclitaxel in pulmonary adenocarcinoma. N Engl J Med 2009;361:947–57.
9. Maemondo M, Inoue A, Kobayashi K, Sugawara S, Oizumi S, Isobe H, et al. Gefitinib or chemotherapy for non-small-cell lung cancer with mutated EGFR. N Engl J Med 2010;362:2380–8.
10. Mitsudomi T, Morita S, Yatabe Y, Negoro S, Okamoto I, Tsurutani J, et al. Gefitinib versus cisplatin plus docetaxel in patients with non-small-cell lung cancer harbouring mutations of the epidermal growth factor receptor (WJTOG3405): an open label, randomised phase 3 trial. Lancet Oncol 2010;11:121–8.
11. John T, Liu G, Tsao MS. Overview of molecular testing in non-small-cell lung cancer: mutational analysis, gene copy number, protein expression and other biomarkers of EGFR for the prediction of response to tyrosine kinase inhibitors. Oncogene 2009;28 Suppl 1:S14–23.
12. Burris HA III. Shortcomings of current therapies for non-small-cell lung cancer: unmet medical needs. Oncogene 2009;28 Suppl 1:S4–13.
13. Vansteenkiste J, Fischer BM, Dooms C, Mortensen J. Positron-emission tomography in prognostic and therapeutic assessment of lung cancer: systematic review. Lancet Oncol 2004;5:531–40.
14. Stroobants S, Goeminne J, Seegers M, Dimitrijevic S, Dupont P, Nuyts J, et al. 18FDG-Positron emission tomography for the early prediction of response in advanced soft tissue sarcoma treated with imatinib mesylate (Glivec). Eur J Cancer 2003;39:2012–20.
15. Jager PL, Gietema JA, van der Graaf WT. Imatinib mesylate for the treatment of gastrointestinal stromal tumours: best monitored with FDG PET. Nucl Med Commun 2004;25:433–8.
16. Su H, Bodenstein C, Dumont RA, Seimbille Y, Dubinett S, Phelps ME, et al. Monitoring tumor glucose utilization by positron emission tomography for the prediction of treatment response to epidermal growth factor receptor kinase inhibitors. Clin Cancer Res 2006;12:5659–67.
17. Sunaga N, Oriuchi N, Kaira K, Yanagitani N, Tomizawa Y, Hisada T, et al. Usefulness of FDG-PET for early prediction of the response to gefitinib in non-small cell lung cancer. Lung Cancer 2008;59:203–10.
18. Nagai Y, Miyazawa H, Huqun, Tanaka T, Udagawa K, Kato M, et al. Genetic heterogeneity of the epidermal growth factor receptor in non-small cell lung cancer cell lines revealed by a rapid and sensitive detection system, the peptide nucleic acid-locked nucleic acid PCR clamp. Cancer Res 2005;65:7276–82.
19. Inohara H, Enomoto K, Tomiyama Y, Higuchi I, Inoue T, Hatazawa J. Impact of FDG-PET on prediction of clinical outcome after concurrent chemoradiotherapy in hypopharyngeal carcinoma. Mol Imaging Biol 2010;12:89–97.
20. Therasse P, Arbuck SG, Eisenhauer EA, Wanders J, Kaplan RS, Rubinstein L, et al. New guidelines to evaluate the response to treatment in solid tumors. European Organization for Research and Treatment of Cancer, National Cancer Institute of the United States, National Cancer Institute of Canada. J Natl Cancer Inst 2000;92:205–16.
21. Antoch G, Kanja J, Bauer S, Kuehl H, Renzing-Koehler K, Schuette J, et al. Comparison of PET, CT, and dual-modality PET/CT imaging for monitoring of imatinib (STI571) therapy in patients with gastrointestinal stromal tumors. J Nucl Med 2004;45:357–65.
22. Young H, Baum R, Cremerius U, Herholz K, Hoekstra O, Lammertsma AA, et al. Measurement of clinical and subclinical tumour response using [18F]-fluorodeoxyglucose and positron emission tomography: review and 1999 EORTC recommendations. European Organization for Research and Treatment of Cancer (EORTC) PET Study Group. Eur J Cancer 1999;35:1773–82.

Published OnlineFirst October 21, 2011; DOI:10.1158/1078-0432.CCR-11-0868

23. Svanholm H, Starklint H, Gundersen HJ, Fabricius J, Barlebo H, Olsen S. Reproducibility of histomorphologic diagnoses with special reference to the kappa statistic. APMIS 1989;97:689–98.
24. Lee ET, Go OT. Survival analysis in public health research. Annu Rev Public Health 1997;18:105–34.
25. Paez JG, Janne PA, Lee JC, Tracy S, Greulich H, Gabriel S, et al. EGFR mutations in lung cancer: correlation with clinical response to gefitinib therapy. Science 2004;304:1497–500.
26. Lynch TJ, Bell DW, Sordella R, Gurubhagavatula S, Okimoto RA, Brannigan BW, et al. Activating mutations in the epidermal growth factor receptor underlying responsiveness of non-small-cell lung cancer to gefitinib. N Engl J Med 2004;350:2129–39.
27. Cappuzzo F, Ciuleanu T, Stelmakh L, Cicenas S, Szczesna A, Juhasz E, et al. Erlotinib as maintenance treatment in advanced non-small-cell lung cancer: a multicentre, randomised, placebo-controlled phase 3 study. Lancet Oncol 2010;11:521–9.
28. Cersosimo RJ. Gefitinib: an adverse effects profile. Expert Opin Drug Saf 2006;5:469–79.
29. Zander T, Scheffler M, Nogova L, Kobe C, Engel-Riedel W, Hellmich M, et al. Early prediction of nonprogression in advanced non-small-cell lung cancer treated with erlotinib by using [(18)F]fluorodeoxyglucose and [(18)F]fluorothymidine positron emission tomography. J Clin Oncol 2011;29:1701–8.
30. Mileshkin L, Hicks RJ, Hughes BG, Mitchell PL, Charu V, Gitlitz BJ, et al. Changes in 18F-fluorodeoxyglucose and 18F-fluorodeoxythymidine positron emission tomography imaging in patients with non-small cell lung cancer treated with erlotinib. Clin Cancer Res 2011;17:3304–15.
31. Aukema TS, Kappers I, Olmos RA, Codrington HE, van Tinteren H, van Pel R, et al. Is 18F-FDG PET/CT useful for the early prediction of histopathologic response to neoadjuvant erlotinib in patients with non-small cell lung cancer? J Nucl Med 2010;51:1344–8.
32. Shields AF, Mankoff DA, Link JM, Graham MM, Eary JF, Kozawa SM, et al. Carbon-11-thymidine and FDG to measure therapy response. J Nucl Med 1998;39:1757–62.
33. Goerres GW, Stupp R, Barghouth G, Hany TF, Pestalozzi B, Dizendorf E, et al. The value of PET, CT and in-line PET/CT in patients with gastrointestinal stromal tumours: long-term outcome of treatment with imatinib mesylate. Eur J Nucl Med Mol Imaging 2005;32:153–62.
34. Prior JO, Montemurro M, Orcurto MV, Michielin O, Luthi F, Benhattar J, et al. Early prediction of response to sunitinib after imatinib failure by 18F-fluorodeoxyglucose positron emission tomography in patients with gastrointestinal stromal tumor. J Clin Oncol 2009;27:439–45.
35. Lee DH, Kim SK, Lee HY, Lee SY, Park SH, Kim HY, et al. Early prediction of response to first-line therapy using integrated 18F-FDG PET/CT for patients with advanced/metastatic non-small cell lung cancer. J Thorac Oncol 2009;4:816–21.
36. Meissner HH, Soo Hoo GW, Khonsary SA, Mandelkern M, Brown CV, Santiago SM. Idiopathic pulmonary fibrosis: evaluation with positron emission tomography. Respiration 2006;73:197–202.

ANTICANCER RESEARCH *31*: 4665-4672 (2011)

Low Dihydropyrimidine Dehydrogenase Correlates with Prolonged Survival in Patients with Lung Adenocarcinoma Treated with 5-Fluorouracil

YASUSHI SHINTANI[1], MASAYOSHI INOUE[1], YASUNOBU FUNAKOSHI[2], AKIHIDE MATSUMURA[3], MITSUNORI OHTA[4], HAJIME MAEDA[2] and MEINOSHIN OKUMURA[1]

[1]*Department of Thoracic Surgery, Osaka University Graduate School of Medicine, Osaka, Japan;*
[2]*Department of General Thoracic Surgery, National Hospital Organization Toneyama Hospital, Osaka, Japan;*
[3]*Department of General Thoracic Surgery, National Hospital Organization Kinki Chuo Chest Medical Center, Osaka, Japan;*
[4]*Department of General Thoracic Surgery, Osaka Prefectural Medical Center for Respiratory and Allergic Disease, Osaka, Japan*

Abstract. *Background: The enzyme dihydropyrimidine dehydrogenase (DPD) is involved in the metabolism of 5-fluorouracil (5-FU). The aim of this study was to clarify the correlation between the expression of DPD and the efficacy of 5-FU therapy in patients with lung adenocarcinoma (AD). Patients and Methods: We examined surgically resected specimens from 90 stage I to IIIA patients with lung ADs to determine the level of intra-tumoral DPD mRNA. Results: Administration of 5-FU improved the prognosis of patients with low DPD-expressing tumors, whereas it did not do so for patients with high DPD expressing tumors. Patients with low DPD-expressing tumors administered with 5-FU had a significantly better prognosis than those who underwent surgery alone. A Cox proportional hazards regression model revealed that administration of 5-FU was an independent variable to predict prognosis in patients with low DPD-expressing tumors. Conclusion: Quantification of DPD mRNA levels is useful for determining the subgroup of lung AD patients who would benefit most from 5-FU after surgery.*

5-Fluorouracil (5-FU) and its derivatives are widely used for treatment of various types of cancer (1). A recent study showed that postoperative oral administration of tegafur-uracil (UFT) improves survival in patients following resection of stage I lung adenocarcinoma (AD) and its administration has become standard therapy after curative resection in early non-small cell lung cancer (NSCLC) cases (2, 3). Furthermore, a novel oral form of fluorouracil S-1 was shown to have promising effects against advanced NSCLC (4). These findings indicate that 5-FU is effective for NSCLC patients and highlight the importance of detection of biomarkers for prediction of its efficacy for treating NSCLC.

Thymidylate synthase (TYMS), the target enzyme for 5-FU, catalyzes an important process for DNA biosynthesis (5, 6) and we previously reported that the prognosis of NSCLC patients is related significantly to the intratumoral *TYMS* mRNA level (7). Dihydropyrimidine dehydrogenase (DPD) is one of the key enzymes involved in the catabolism of 5-FU and its expression was found useful in predicting the efficacy of 5-FU after surgery for NSCLC based on disease-free interval during short follow-up periods (8-10). In the present study, we examined the efficacy of 5-FU in association with DPD expression in regards to prognosis, including overall survival, in patients with lung ADs over a longer follow-up period.

Patients and Methods

Ninety specimens from lung AD patients determined to be p-stage I to IIIA were obtained during surgical procedures at Osaka University Hospital, Kinki Chuo Chest Medical Center, Toneyama Hospital, and Osaka Prefectural Medical Center for Respiratory and Allergic Disease between January 1999 and March 2003. Quantification of *TYMS* and *DPD* mRNA levels in AD tissues was performed as described previously (7, 10). The obtained copy numbers of *TYMS* and *DPD* were standardized with glyceralde-hydo-3-phosphate dehydrogenase (*GAPDH*) mRNA quantity, used as an endogenous control, with the following equation: 'Result'=Log (*TYMS* or *DPD* RNA copy number in tumor)/(*GAPDH* RNA copy number in tumor)×(6.1×10^9; *GAPDH* RNA copy number in 1 μg of total RNA extracted from the peripheral blood of 30 healthy volunteers).

Correspondence to: Yasushi Shintani, MD, Ph.D., Department of General Thoracic Surgery, Osaka University Graduate School of Medicine, 2-2-L5, Yamadaoka, Suita-city, Osaka, 565-0871, Japan. Tel: +81 668793152, Fax: +81 668793164, e-mail: yshintani@thoracic.med.osaka-u.ac.jp

Key Words: Lung adenocarcinoma, 5-fluorouracil, dihydropyrimidine dehydrogenase, thymidylate synthase, chemosensitivity.

Table I. *Patient background data.*

Variable	Treatment		
	Surgery alone (control) n=60	5-FU n=30	*p*-Value
Age (years)	63±9.3	62±9.4	0.445
Gender			
Male	35 (58%)	20 (67%)	0.426
Female	25 (42%)	10 (33%)	
Pathologic stage			
I	38 (63%)	20 (67%)	
II	9 (15%)	6 (20%)	0.882
IIIA	13 (22%)	4 (13%)	

5-FU, 5-fluorouracil. *p*-Value, chi-square test or Mann-Whitney *U*-test.

Table II. *Thymidylate synthase (TYMS) and Dihydropyrimidine dehydrogenase (DPD) mRNA levels, and clinicopathologic factors.*

Factor	n	Log TYMS mRNA	*p*-Value	Log DPD mRNA	*p*-Value
Tumor status			0.029		0.054
pT1	49	6.90±0.29		6.89±0.48	
pT2	36	7.03±0.33		6.63±0.54	
pT3	5	7.42±0.54		6.99±0.27	
Nodal status			0.600		0.546
pN0	61	6.96±0.34		6.80±0.57	
pN1	12	7.00±0.36		6.75±0.41	
pN2	17	7.04±0.35		6.80±0.33	

p-Value, chi-square test or Mann-Whitney *U*-test.

Informed consent was obtained from all patients. Those administered UFT following surgery comprised the 5-FU group (n=30), while those who underwent surgery only, comprised the control group (n=60). UFT administration was started within 2 months after surgery and continued for more than 12 months. The dose of UFT was 300-400 mg/day and the mean duration of treatment was 21.5±7.3 months (mean±SD; range 12-26 months). The clinical backgrounds of the patients are summarized in Table I. There was no difference in clinical factors between the groups. The median follow-up period was 78±23 months (range 17-115 months) after surgery.

Chi-square, Mann-Whitney *U*, and Kruskal-Wallis tests were used to compare the results, while survival rates were estimated by the method of Kaplan and Meier and compared using log-rank test, using Statview version 5.0 for Windows (Abacus Concepts, Berkeley, CA, USA). A *p*-value of <0.05 was considered to be statistically significant.

Results

Quantification of *TYMS* and *DPD* mRNA levels in NSCLC tissues was successfully performed for all specimens. Intratumoral *TYMS* and *DPD* mRNA levels ranged from 6.28 to 8.04 (mean±SD; 6.98±0.34) and 5.36 to 8.28 (6.79±0.59), respectively. The results for *TYMS* and *DPD* mRNA levels are summarized in Table II. *TYMS* mRNA levels were associated with tumor status, while *DPD* mRNA levels were not associated with tumor or nodal status.

Thirty-five (39%) of the 90 patients developed distant metastasis after surgery. In regards to tumor stage, 12 (21%) out of 58 patients in stage I, 8 (53%) out of 15 patients in stage II, and 15 (88%) out of 17 patients in stage IIIA suffered from recurrent disease. Categorized by group, 27 (45%) out of 60 patients and 8 (27%) out of 30 in the control and 5-FU groups, respectively, had recurrence. There was no significant difference in overall survival rate between the groups (Figure 1A). Similar to a previous report (7), *TYMS* mRNA levels were significantly correlated to overall survival when dichotomized at the mean *TYMS* mRNA level (Figure 1B).

Next, we evaluated the correlation between *DPD* expression and efficacy of 5-FU. *DPD* mRNA levels were significantly correlated to overall survival in the 5-FU group, but not in the control group when dichotomized at the mean *DPD* mRNA level (Figure 2). In the 5-FU-group, the 5-year survival rate was 92% for the low DPD-expressing subgroup and 68% for the high DPD-expressing subgroup. Patients with low DPD-expressing tumors, who were administered 5-FU had a significantly better prognosis than those who underwent surgery alone (Figure 3A); the 5-year survival rates were 92% for the 5-FU group and 53% for the control group. These findings suggest that the intratumoral *DPD* mRNA level may be a possible predictor for efficacy of 5-FU administration after surgery for NSCLC. On the other hand, patients with high DPD-expressing tumors administered 5-FU had a tendency for a worse prognosis as compared to those who underwent surgery alone (Figure 3B).

We analyzed 5 variables, namely tumor status, nodal metastasis, *TYMS* mRNA expression, *DPD* mRNA expression, and 5-FU administration, using a Cox proportional hazards regression model to determine their effects on overall survival in NSCLC patients (Table IIIA). Multivariate analysis revealed that p-N2 and *TYMS* mRNA expression were independent variables for predicting overall survival (Table IIIB). Furthermore, in patients with low DPD-expressing tumors, multivariate analysis showed that *TYMS* mRNA expression and administration of 5-FU, were each independent variables predicting prognosis (Table IIIC).

Discussion

We performed quantitative assays of intratumoral *TYMS* and *DPD* mRNA levels to assess their association with clinicopathological factors, as well as the feasibility of applying them to predict the efficacy of 5-FU therapy in